Surveys in Geophysics (2022) 43:913–957
https://doi.org/10.1007/s10712-022-09705-4

Geophysical Well-Log Evaluation in the Era of Unconventional Hydrocarbon Resources: A Review on Current Status and Prospects

Jin Lai[1,2] · Guiwen Wang[1,2] · Qixuan Fan[2] · Xiaojiao Pang[2] · Hongbin Li[2] · Fei Zhao[2] · Yuhang Li[2] · Xin Zhao[2] · Yidi Zhao[2] · Yuyue Huang[2] · Meng Bao[2] · Ziqiang Qin[3] · Qiqi Wang[4]

Received: 20 December 2021 / Accepted: 24 March 2022 / Published online: 29 April 2022

Abstract
Geophysical well-log evaluation in the era of unconventional hydrocarbon resources (mainly tight oil and gas, shale oil and gas) is complicated and challenging. This review aims to fill this gap between well-log evaluation and unconventional hydrocarbon resources by characterizing the source rock property, reservoir property and engineering property using petrophysical well logs. The advanced well-log series used for unconventional oil and gas evaluation include nuclear magnetic resonance (NMR) log, image logs, array acoustic logs, elemental capture spectroscopy (ECS) and LithoScanner logs. The source rock property in terms of total organic carbon content is predicted using conventional logs and LithoScanner log. Then petrophysical parameters including porosity, permeability and oil saturation are calculated, and the appearance of natural fracture is predicted from conventional, sonic logs, image logs and NMR logs. Additionally, the reservoir property is evaluated to optimize the favorable layers with high hydrocarbon bearing property and productivity. Brittleness index as well as in situ stress direction and magnitudes are characterized by the comprehensive use of density, sonic log, ECS log and image logs. Then, the engineering property (high brittleness index but low horizontal stress difference) is evaluated to screen out the prospected layers for hydraulic fracturing. The internal relationships between the three types of properties are unraveled, and the geological and engineering sweet spots are optimized by integrating lithology, reservoir quality, hydrocarbon bearing property, source rock property, brittleness and in situ stress magnitude and direction. This multidisciplinary approach provides a comprehensive method for optimizing sweet spots in unconventional play, and will support petroleum geoscientists' and engineers' decisions in exploration and exploitation of unconventional hydrocarbon resources.

Article Highlights

- This paper surveys the current status and prospects of well log evaluation of unconventional oil and gas

✉ Jin Lai
sisylaijin@163.com

Extended author information available on the last page of the article

- Geophysical well log evaluation of unconventional hydrocarbon resources characterizes source rock property, reservoir property and engineering property
- Geological and engineering sweet spots can be optimized by petrophysical and geomechanical properties determined from well logs

Keywords Unconventional hydrocarbon resources · Source rock property · Reservoir property · Engineering property · Sweet spot · Well logs

List of symbols

Well-log curve names:

AC	Sonic interval transit time
AT90, AT60, AT30, AT20, AT10	High definition induction logs
CAL, CALI	Caliper log
CNL	Compensated neutron log
CGR	GR log without *U* contribution
DEN	Bulk density
DT	Sonic transit time log
ECS	Elemental capture spectroscopy
FMI	Fullbore formation microimager
GR	Natural gamma-ray
ILM	Medium induction logs
ILD	Deep induction logs
K, Th, U	Spectral gamma-ray log
KTH	GR log without *U* contribution
LLS, LLD	Shallow and deep lateral log
M2Rx, M2R9, M2R6, M2R3, M2R2, M2R1	High definition induction logs
MSFL	Micro spherically focused log
MSIP	Modular sonic imaging platform
NPHI	Neutron porosity logs
NMR	Nuclear magnetic resonance
Pe	Litho-density
RHOB	Density log
RI	Induction logs
Ro	Vitrinite reflectance
Rxo, Rt	Resistivity of flushed zone and uninvaded zone
SGR	Total gamma-ray log
SP	Spontaneous potential
SFLU	Micro-resistivity log
T_1	Longitudinal relaxation time
T_2	Transversal relaxation time
$T_{2\mathrm{gm}}$	T_2 Weighted mean on a logarithmic scale
$T_{2\mathrm{cutoff}}$	Transition T_2 value separating immobile fluid from mobile fluid

Other Nomenclatures

ANN	Artificial neural network

BVI	Bulk volume irreducible
CT	Computed tomography
ELAN	Quanti elemental log analysis
E	Young's modulus
FFI	FFI free fluid index
MICP	Mercury injection capillary pressure
RQI	Reservoir quality index
SDR	Schlumberger-Doll research
SEM	Scanning electron microscopy
Sh	Hydrocarbon saturation
Sv	Vertical stress
SHmax	Magnitudes of maximum horizontal stress
Shmin	Minimum horizontal stress
S_1	Volatile hydrocarbon
S_2	Remaining hydrocarbon
SVM	Support vector machine
TOC	Total organic carbon
TIC	Total inorganic carbon
TC	Total carbon
v	Poisson's ratio
φ	Porosity
K	Permeability

1 Introduction

Unconventional hydrocarbon resources, which mainly include tight and shale oil and gas, etc., play more and more important roles in the world energy structure (Zou et al. 2019; Nikolaev and Kazak 2019; Wu et al. 2019; Amosu et al. 2021; Mukhametdinova et al. 2021). The increasing market demand and technological advances in directional geosteering, horizontal drilling and multi-stage hydraulic fracturing have made unconventional plays a major focus for the global petroleum industry (Qiu et al. 2016; Curtis et al. 2012; Rybacki et al. 2016; Iqbal et al. 2018; Sun et al. 2021). However, unconventional tight to shale reservoirs have varied lithologies (structure and composition) (Chen et al. 2017; Cao et al. 2017; Li Maowen et al. 2019), ultra-low permeability (Gale et al. 2007; Josh et al. 2012; Avanzini et al. 2016; Bai et al. 2017) and the pore systems are dominated by highly heterogeneous nano- to microscale pore assemblages (Curtis et al. 2012; Loucks et al. 2012; Manjunath and Jha 2019; Chandra and Vishal 2021). Therefore, unconventional reservoirs commonly have remarkably different well-log responses compared with conventional reservoirs (Iqbal et al. 2018), and formation evaluation for unconventional plays using petrophysical well logs remains complicated and challenging (Du et al. 2021; Amosu et al. 2021; Liu 2021).

Source rock property needs to be evaluated via well logs for the self-sourced and self-retained unconventional resources (Zhao et al. 2019). Reservoir quality is also one of the key risk factors for productivity (Zhang et al. 2015; Mukhametdinova et al. 2021). In addition, unconventional reservoirs have no natural productivity, and therefore, hydraulic fracturing is required for the economic production (Gale et al. 2007; Josh et al. 2012; Avanzini et al. 2016; Dong et al. 2018; Manjunath and Jha 2019). Consequently, the engineering property (brittleness and in situ stress states) has become critical petrophysical parameters for screening prospected layers for hydraulic fracturing (Lai et al. 2015; Iqbal et al. 2018).

The optimization of "sweet spots" (hydrocarbon-rich zones with matured high-quality source rocks, favorable reservoir quality and prospected layers for stimulation) integrating source rock property, reservoir property and engineering property is essential for exploitation of unconventional resources (Zou et al. 2013; Lu et al. 2019). Petrophysical well logs, when calibrated with core analysis data, have the advantages for continuous evaluation of source rock property, reservoir property and engineering property of unconventional plays with low cost (Clarkson et al. 2012; Avanzini et al. 2016; Iqbal et al. 2018).

Due to the fundamental difference in petrophysical and geomechanical properties of unconventional plays, a systematic workflow is required to characterize the seven kinds of parameters (lithology, reservoir quality, hydrocarbon bearing property, electronic well-log responses, source rock property, brittleness and in situ stress magnitude and direction) and the three kinds of properties (source rock property, reservoir property and engineering property) (Zou et al. 2019; Mukhametdinova et al. 2021). This review aims to fill the gap between geological and petrophysical characterization of unconventional resources, and the different types of logs from the Ordos Basin, the Subei Basin, the Junngar Basin and the Tarim Basin are used. Firstly, the commonly used geophysical well-log series are reviewed. Secondly, the source rock property in terms of TOC abundance is evaluated using conventional, spectrum gamma-ray and LithoScanner logs. Thirdly, the reservoir property in terms of lithology, porosity, permeability, oil saturation and the presences of fractures is predicted by conventional, sonic logs, image logs and NMR logs. Fourthly, the engineering property in terms of in situ stress direction and magnitudes as well as brittleness index is characterized by sonic logs and image logs. Lastly, the geological and engineering sweet spots optimization is performed by unraveling the relationships between three types of properties. This study critically reviews the petrophysical well-log evaluation of unconventional resources, as assessed from peer reviewed papers and from the authors' personal experiences, with the aim that readers can use these results for their future work.

2 Geophysical Well-Log Series

A series of geophysical well-log suits spanning from conventional well logs to advanced well-log suits, which have varied vertical resolution and depth of investigation, can be used for unconventional oil and gas resource evaluation (Fig. 1) (Yarmohammadi et al. 2020; Mukhametdinova et al. 2021).

Conventional well-log series include caliper (CAL), spontaneous potential (SP), natural gamma-ray (GR), litho-density (Pe), sonic interval transit time or acoustic log (AC), compensated neutron log (CNL) and bulk density (DEN) (Fig. 1). Three resistivity logs can be divided according to their depth of investigation, and micro log (MSFL, MIL) measures the resistivity of mudcake with a depth of investigation of 2.5–10 cm. Lateral logs (LLS, LLD) and induction logs (ILM, ILD) can measure the resistivity of flushed zone (Rxo) and uninvaded zone (Rt) (Fig. 1). In addition, in order to improve the vertical resolution and depth of investigation, high definition induction logs HDIL (M2Rx, M2R9, M2R6, M2R3, M2R2, M2R1), which have a vertical resolution of 1–2 ft, and depths of investigation of 10–120 ft, are developed (Fig. 1).

Electrical or ultrasonic borehole image logs, which measure the electrical resistivity or acoustic impedance of borehole wall (Khoshbakht et al. 2009), provide very high-resolution (5 mm) borehole pictures (Prioul et al. 2007; Folkestad et al. 2012). FMI (fullbore formation microimager) imaging tool, which have 8 pads and each contains 24 buttons, electrically scan the borehole wall, and a total of 192 micro-resistivity curves are collected (Khoshbakht et al. 2009; Rajabi et al. 2010). Then, the micro-resistivity curves are used to build up a "pseudo-picture" of

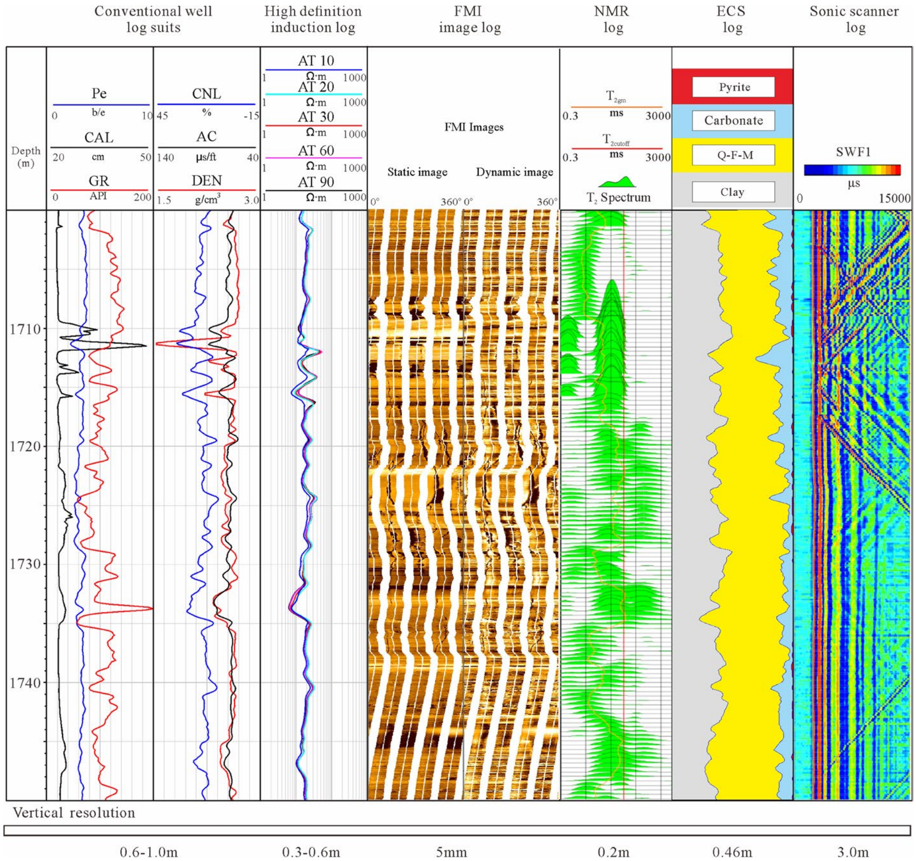

Fig. 1 Conventional geophysical well-log data and advanced well-log suits with various vertical resolutions used in well-log evaluation

the wellbore through speed correction, eccentering correction and normalization (Goodall et al. 1998; Rajabi et al. 2010; Wilson et al. 2013; Keeton et al. 2015). Geological features in terms of fracture, fault, bedding and vug as well as cavity can be picked out from the high-resolution images (Fig. 1) (Xu et al. 2009; Khoshbakht et al. 2012; Lai et al. 2018a; Wang et al. 2020).

Nuclear magnetic resonance (NMR) logging tool measures the longitudinal relaxation time (T_1), transversal relaxation time (T_2) spectrum and diffusion coefficient (D) and has a vertical resolution of 0.2 m (Kleinberg et al. 2005; Tan et al. 2014; Bauer et al. 2015; Liu et al. 2019; Wang et al. 2020). The NMR T_2 spectrum is widely used for fluid property discrimination (Wang et al. 2020), and can be used for determination of porosity, estimation of permeability, evaluating irreducible water saturation and hydrocarbon saturation (Fig. 1) (Dunn et al. 2002; Kleinberg et al. 2005; Hübner 2014; Bauer et al. 2015; Olatinsu et al. 2017). Additionally, plot of T_1 versus T_2 as well as plot of T_2 versus diffusion coefficient can be used for fluid property determination since the hydrocarbon and water signals can be clearly separated due to the large contrast between diffusion coefficients of hydrocarbon and water (Sun and Dunn 2005).

The elemental capture spectroscopy (ECS) and LithoScanner logs with a vertical resolution of 0.457 m (1.5 ft) can directly provide the rock compositions (clay, quartz, feldspar, and mica (Q-F-M), carbonate and pyrite, etc.) (Maliva et al. 2009; Collett et al. 2011), and are widely used for mineral content determination, lithology recognition and even TOC calculation (Fig. 1) (Guo et al. 2019).

Array acoustic logging tools or sonic scanner (MSIP—modular sonic imaging platform) logs, which have a vertical resolution of 3.0 m, measure the full wave-forms including compressional wave slownesses, shear-wave slownesses, Stoneley wave and pseudo-Rayleigh wave (Collett et al. 2011; Zaree et al. 2016). Therefore, sonic logs are widely used in the fields of engineering geology in calculating geomechanical parameters, determining in situ stress and rock anisotropy (Fig. 1) (Liu et al. 2018).

Conventional well logs can be collected in most of the wells, while the advanced well logs (image logs, NMR log, LithoScanner log, array sonic logs) are too expensive, and are not available for all the wells drilled.

3 Source Rock Property

Quality (types), quantity (abundance) and thermal maturity are three important geochemical parameters for source rock evaluation (Zhao et al. 2019). Organic matter abundance (quantity) can be characterized by total organic carbon content (TOC), which is defined as the organic richness or amount of organics within source rocks (Jarvie et al. 2007; Iqbal et al. 2018). Thermal maturity is the degree or stage of organic matters transformation into hydrocarbon at adequate pressure and temperature with increase in burial depth (Zhao et al. 2019). Vitrinite reflectance (Ro, %) is often used as a measure of thermal maturity of source rocks (Zhao et al. 2019). Zhao et al. (2019) integrates resistivity, neutron and density logs to estimate thermal maturity index for Barnett shale.

3.1 Well-log Responses of Source Rocks

Shales have distinct responses in well logs due to the unique physical properties of the organic matters (Aziz et al. 2020). Source rocks are organic matter-rich mudstones/shales, which can be qualitatively recognized by conventional well logs due to their distinct petrophysical properties compared with reservoir rocks. Mudstones and shales are inherently different from sandstones or carbonate rocks due to their high gamma-ray; additionally, the presences of organic matters will amplify this effect (Aziz et al. 2020). Conventional well-log series which are sensitive to organic matters include gamma-ray (GR), sonic transit interval time (AC), neutron porosity (CNL), bulk density (DEN) and resistivity (RT) (Wang et al. 2019; Aziz et al. 2020).

GR tool measures the radioactivity, and the presence of organic matter-rich source rocks will cause intense radioactivity and consequently high GR values (Shalaby et al. 2019). For instance, the source rocks in Yanchang Formation Member 7 of Ordos Basin, West China, have high GR readings (Fig. 2). The anomalously high GR was mainly ascribed to uranium, which is related to the organic matter (Fig. 2) (Wang et al. 2019).

Mudstones conventionally show high AC values than sandstones, and transit interval time of organic matters (about 500 μs/m) is much larger than that of rock matrix. Therefore, organic matter-rich source rocks will show much higher AC logging values (Fig. 2) (Wang et al. 2019).

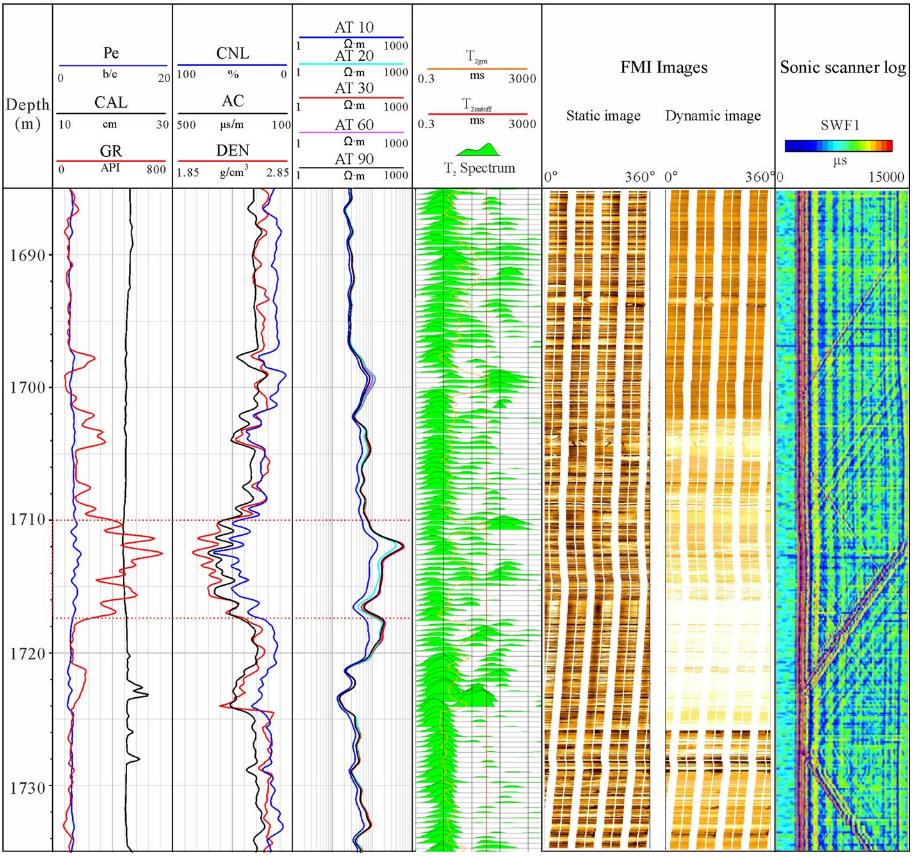

Fig. 2 Well-log responses of source rocks in Yanchang Formation Member 7 of Ordos Basin, West China

Neutron log measures the hydrogen index in rocks (Shalaby et al. 2019). Organic matters commonly have high hydrogen index, which gives high neutron porosity logging (CNL) value (Fig. 2) (Wang et al. 2019).

Density log is the comprehensive reflection of fluids and matrix components (Shalaby et al. 2019). Organic matters (kerogen) have much lower bulk density (about 1.0 g/cm^3) than the matrix rocks (2.5–2.7 g/cm^3); consequently, the density log value will significantly decrease when encountered with source rocks (Fig. 2) (Wang et al. 2019; Shalaby et al. 2019).

The mudstone intervals generally exhibit low resistivity because of the good conductivity of clay minerals and pore water. However, the organic matter-rich mudstones (shales) are non-conductive; additionally, in mature source rocks, the non-conductive hydrocarbon will further cause a high anomaly in the resistivity logs (Passey et al. 1990; Wang et al. 2019; Shalaby et al. 2019; Wood 2020a). The high definition resistivity log (AT10-AT90) shows abnormally high readings and is deviated evidently in the source rock intervals (Fig. 2) (Shalaby et al. 2019).

In Fig. 2, the source rocks are therefore evidently recognized in the 1710–1718 m depth intervals and are characteristic of abnormal high GR readings, low bulk density, but high sonic transit time, high neutron porosity and high resistivity (Fig. 2). The image logs are white due to the high resistivity and abundant lamina is recognized. The NMR logs and array acoustic logs show no evident responses in the source rock intervals (Fig. 2).

3.2 TOC Prediction via Well Logs

TOC, volatile hydrocarbon (S_1) and remaining hydrocarbon (S_2), which reflect richness and hydrocarbon generation potential of organic matters, are three significant factors for source rock property evaluation (Aziz et al. 2020). The content of S_1 and S_2 estimations can be processed through regression analysis between TOC and (S_1+S_2) content (Wang et al. 2019). TOC is the organic richness or amount of organics within rock (Jarvie et al. 2007; Iqbal et al. 2018). TOC value can be accurately measured using rock pyrolysis (Iqbal et al 2018); however, core data are not available in all intervals or wells due to high cost and low recovery rate (Aghli et al. 2016; Lai et al. 2017). Therefore, TOC estimation using well logs is vital for continuous evaluation of source rock property. There are various methods proposed to calculate TOC using well logs, including (1) Δlog*R* method, (2) spectral gamma-ray log, (3) multivariate fitting method and (4) advanced log method (LithoScanner log), (5) machine Learning (learning) method, etc.

3.2.1 Δlog*R* Method

The ΔlogR method was initially proposed by Passey et al. (1990), and had been widely used for TOC estimation using well logs in carbonates and clastic rocks. Δlog*R*, i.e., the sonic-resistivity overlay plot AC and true formation resistivity Rt logs in one track, additionally AC and RT are scaled as a ratio of 50 μs/ft to one resistivity cycle. The separation between two curves (AC to the left and RT to the right) is defined as Δlog*R* (Passey et al. 1990; Shalaby et al. 2019). The AC curve will reflect low density/low velocity kerogens, while the Rt curve will respond to formation fluid (Tenaglia et al. 2020).

The method of sonic-resistivity overlay (Δlog*R*) is used to calculate TOC content (Eqs. 1, 2).

$$\Delta \log R = \log(R/R_{\text{Baseline}}) + 0.02(\Delta t - \Delta t_{\text{Baseline}}) \tag{1}$$

$$\text{TOC} = \Delta \log R \times 10^{(2.297-0.1688LOM)} \tag{2}$$

R is deep resistivity log (Ω m^{-1}), and the RT and LLD logs can be used; Δ*t* (AC) is the sonic transit time (μs/ft or μs/m), almost all suits of logs give the AC curve; R_{Baseline} and $\Delta t_{\text{Baseline}}$ are the resistivity and sonic transit time values at the base line; LOM (local level of organic metamorphism) is a constant related to thermal maturity. In some cases, sonic transit time curve may not be unavailable, and then, density or neutron log can be used instead (Shalaby et al. 2019; Tenaglia et al. 2020).

The scaling of sonic and resistivity well logs during overlaying is set as a ratio of − 164 μs/m (− 50 μs/ft) sonic transit time (Δ*t*) to one logarithm resistivity cycle Ω m^{-1} (for instance, 1–10 Ω m^{-1}) (Passey et al. 1990; Iqbal et al. 2018; Godfray and Seetharamaiah 2019; Wang et al. 2019; Shalaby et al. 2019). The TOC can be calculated using the above Δlog*R* method providing that the baseline of AC and RT is determined. The TOC predicted from Δlog*R* methods is in accordance with the core-measured TOC content in Lucaogou Formation of Jimusar Sag, Junggar Basin, West China (Fig. 3). Then, the TOC

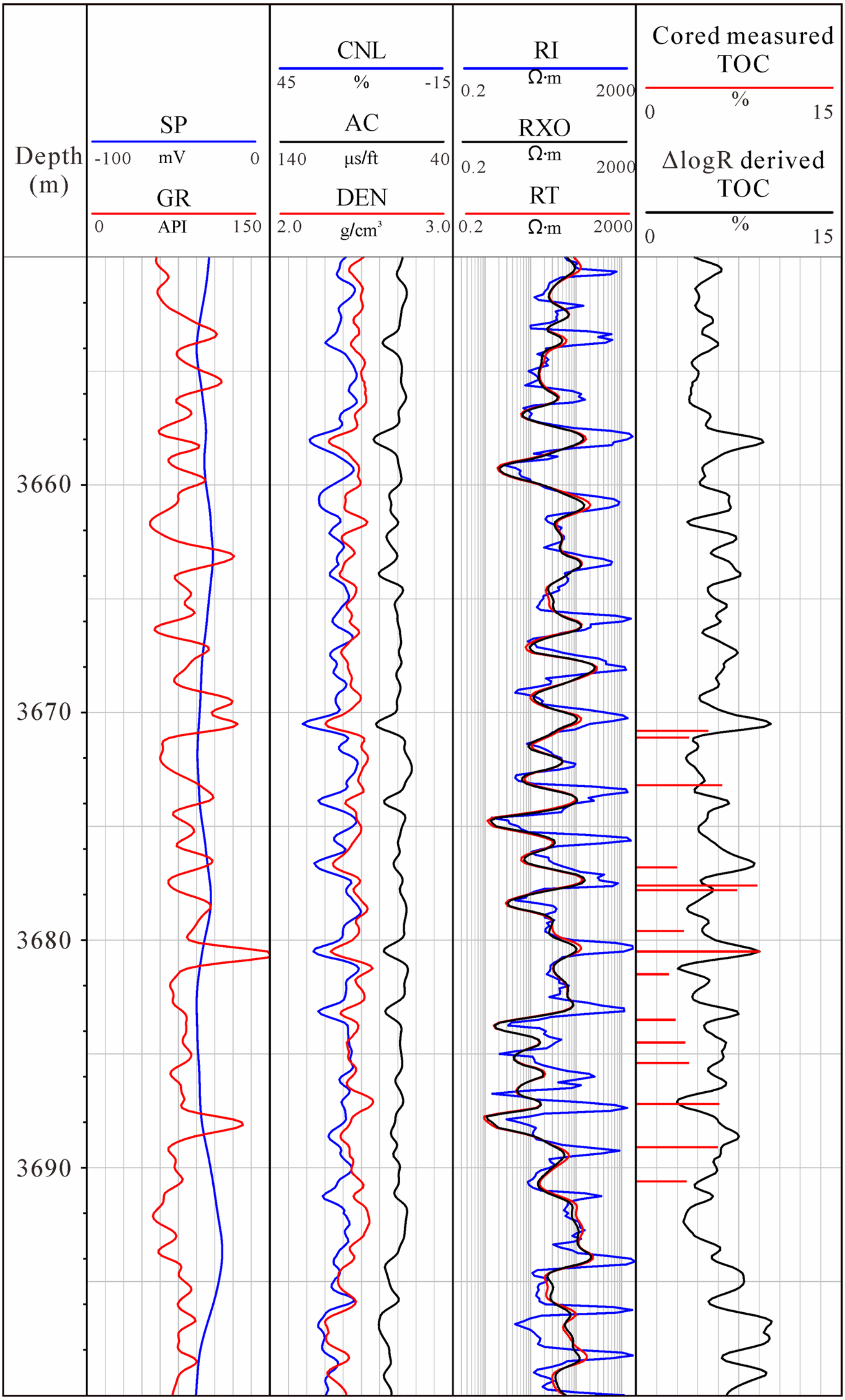

Fig. 3 TOC estimation using ΔlogR method in Lucaogou Formation of Jimusar Sag, Junggar Basin, West China

content is estimated using the above formula, and the results are in accordance with core-measured TOC content (Fig. 3).

Source rock intervals can be firstly qualitatively identified using GR, CNL, DEN and resistivity log curves. Additionally, plotted AC and RT in one track with scaling of 100 μs/ft (for instance 140–40 μs/ft) transit time to two logarithm resistivity cycle (10–1000 Ω m^{-1}) also give the source rock intervals. As is known, AC and RT logs will overlap with each other in non-source rock interval, while the two logs will deviate evidently at the source rock intervals. There are many Δ*LogR*-based methods widely used to estimate TOC content using well logs (Zhao et al. 2016).

The limitation of Δlog*R* is that the baselines vary from formation to formation and well to well (Wang et al. 2019). Additionally, the presence of pyrite will mask resistivity profile and show low resistivity (Passey et al. 1990; Iqbal et al. 2018).

3.2.2 Spectral Gamma-Ray Log

GR logging tool measures the total intensity of radioactivity of formation which come from K, Th and U elements. GR spectrometer allows to detect the individual concentrations of K (%), U (ppm) and Th (ppm) (Sérgio et al. 2018). Spectral gamma-ray logs are therefore widely used for estimating clay content, paleoclimate reconstruction grain size evaluation (Sérgio et al. 2018). Organic matters can absorb abundant U elements, and therefore, U log curve or KTH (GR log without U contribution) can be used for TOC estimation. As can be observed in Fig. 4, in Funing Formation in Subei Basin, East China, the TOC value shows negative relationship with KTH log with high correlation coefficient (Fig. 4).

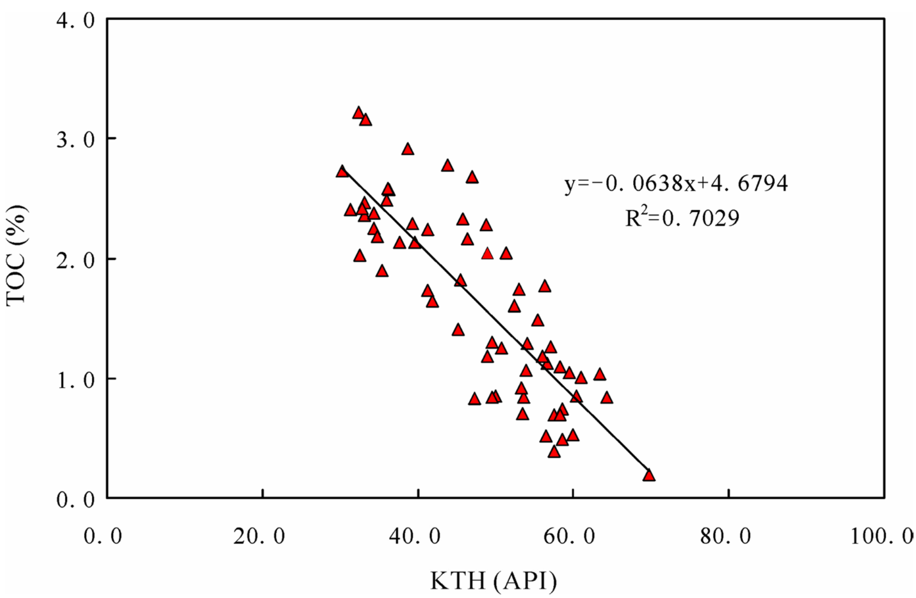

Fig. 4 Crossplot of KTH versus core-measured TOC content of Funing Formation in Subei Basin, East China. KTH is the GR log without U contribution derived from spectral gamma-ray log

3.2.3 Multivariate Fitting Method

The multivariate fitting method is integrating two or more log curves which are sensitive to the source rocks to establish a model to calculate TOC (Aziz et al. 2020). For instance, the model used to estimate TOC using well logs can be written as the following Eq. (3) through multivariate fitting method. Consequently, the TOC content in well intervals can be predicted, and the results are in good accordance with core-measured TOC (Fig. 5).

$$TOC = 0.0194GR + 3.582AC - 0.0051LLD - 8.124DEN - 175.352 \quad (3)$$

3.2.4 LithoScanner Logs

The LithoScanner logging technology, which was proposed by Schlumberger Company, is the improvement of elemental capture spectroscopy (ECS) log (Guo et al. 2019). LithoScanner logs can measure the content of common elements including carbon, potassium, magnesium, aluminum and sodium (Guo et al. 2019). Through data processing, the element content can be transformed into the mineralogy content, including clay, Q–F–M (quartz–feldspar–mica), carbonate (calcite and dolomite) and pyrite (Fig. 1). Consequently, the ECS and LithoScanner logs are widely used for mineral composition determination, lithology recognition or even brittleness index evaluation (Maliva et al. 2009; Collett et al. 2011; Lai et al. 2015).

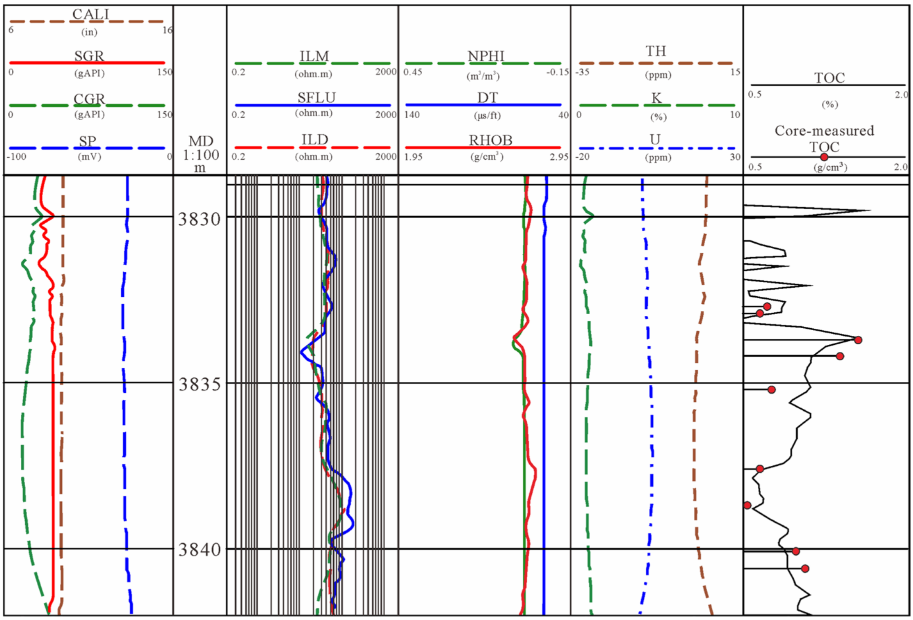

Fig. 5 TOC content calculated from multivariate fitting method in Tarim Basin, West China

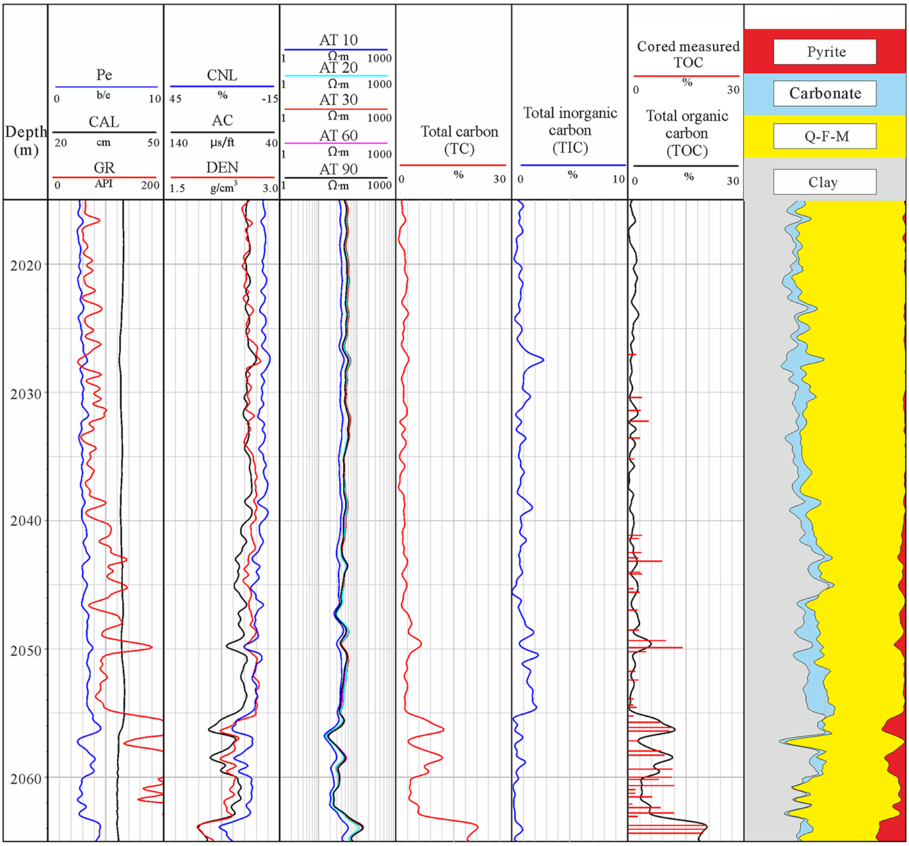

Fig. 6 TOC content calculated from LithoScanner log in Yanchang Formation Member 7 of Ordos Basin, West China

LithoScanner provides the total carbon element (TC) content; however, there is also inorganic carbon (TIC) in the formation (Fig. 6). In hydrocarbon reservoirs, the inorganic carbon is mainly associated with carbonate rocks (Ca_2CO_3, $Ca(Mg)CO_3$, etc.). Consequently, the TOC content can be obtained, providing that the inorganic carbon content is eliminated (Fig. 6). The TOC content calculated from LithoScanner log in Yanchang Formation Member 7 of Ordos Basin is consistent with the core analysis data (Fig. 6).

3.2.5 Machine Learning Methods

The relationships between TOC and logs (GR, AC, DEN, RT, etc.) are complicated and nonlinear; therefore, machine learning methods should be integrated to predict TOC content (Mahmoud et al. 2017; Wang et al. 2019). Wang et al. (2019) uses the artificial neural network (ANN) method to predict TOC content using AC and DEN logs, which improve the efficiency. The support vector machine (SVM) method can also be adopted in TOC prediction via GR, AC and DEN logs (Amosu and Sun 2021). The machine learning methods have the advantages of high accuracy (Mahmoud et al. 2017; Amosu and Sun 2021).

4 Reservoir Property

Reservoir property evaluation aims at characterizing the lithology, porosity (φ), permeability (K) and hydrocarbon saturation (Sh). Conventional (full suite) logs can be used for calculation of these petrophysical parameters for conventional hydrocarbon reservoirs (Yarmohammadi et al. 2020). However, advanced well-log suits including LithoScanner logs, image logs, NMR logs and sonic array logs are required to evaluate the reservoir property (lithology, reservoir quality, fracture, as well as oil bearing property) for unconventional reservoirs due to the complex pore assemblage and petrophysical log responses (Rybacki et al. 2016; Avanzini et al. 2016; Iqbal et al. 2018; Zhao et al. 2019; Yarmohammadi et al. 2020; Liu 2021).

4.1 Well-Log Responses of Oil and Water Bearing Layers

The dry layers (non-reservoir intervals) of Yanchang Formation Member 7 in Ordos Basin have low porosity as can be evidenced by the three porosity logs, and no evident deviations of the deep (AT60–AT90) and shallow (AT10–AT20) induction logs (Fig. 7). Reservoir layers are characterized by high reservoir quality. As can be observed in Layer 1 and Layer 2 in Fig. 7, the high sonic transit time, high CNL but low bulk density gives signatures of

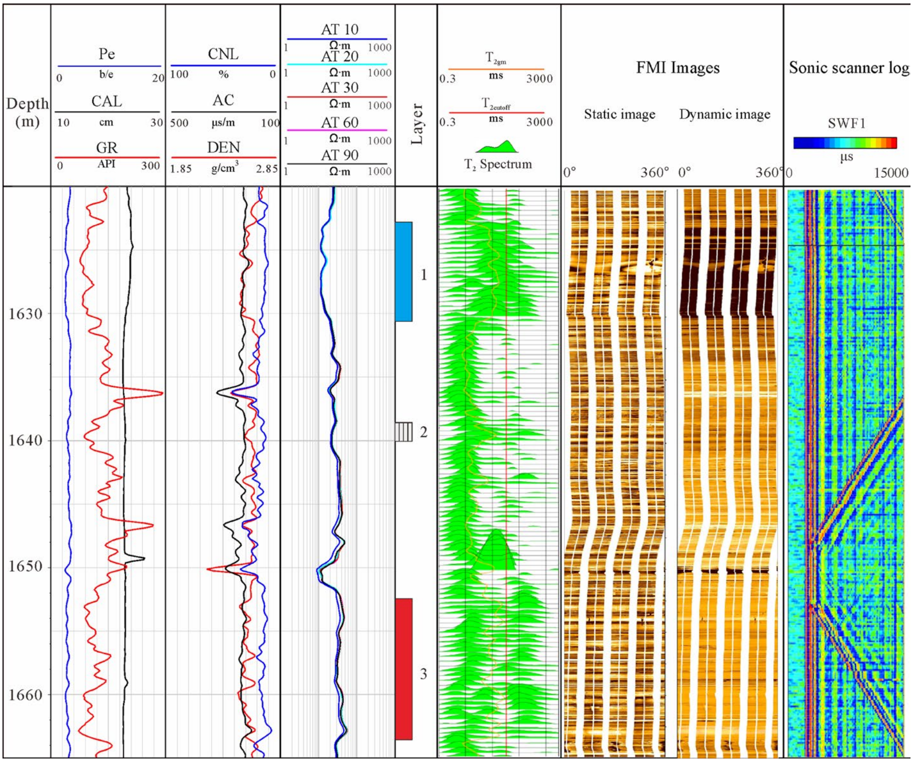

Fig. 7 Well-log responses of typical reservoirs (water and oil bearing layer) in Yanchang Formation Member 7 of Ordos Basin, West China

high reservoir quality (Fig. 7). However, the reservoirs can be water saturated and oil saturated, and the water bearing layers commonly have no deviations of resistivity logs with various depth of investigation (Fig. 7). Conversely, the oil bearing layers are recognized by evident deviations in deep (AT60–AT90) and shallow (AT10–AT20) resistivity logs (Liu et al. 2020) (Fig. 7).

Additionally, NMR logs can also be used for of the fluid type identification and estimation of fluid volumes (Anand 2017). Typical oil bearing layers have high T_2 amplitudes and wide T_2 spectrum or even contain tail distribution (Fig. 7) (Liu et al. 2020). Water bearing layers are characterized by low T_2 amplitudes and have narrow T_2 spectrum, containing no tail distributions (Fig. 7) (Liu et al. 2020). The T_2 spectrum of dry layer is very narrow and the T_2 amplitudes are low (Fig. 7).

4.2 Lithology

The unconventional hydrocarbon resources are mainly reserved in the fine-grained sedimentary rocks, which consist of carbonate, silt and clay (Zhao et al. 2019; Yang et al. 2019). In shale reservoirs, the various mineral compositions including felsic, clay, carbonate or even organic matters can form a complex lamina assemblage (Zhao et al. 2019; Wang et al. 2021). The complexity of unconventional resources requires an accurate evaluation of a petrophysical model for lithology prediction (Stadtmuller et al. 2018). Mudstone/shales mainly constitute the source rock intervals, while the interbedded thin layer of siltstone and/or carbonate rocks with a wide range of pore spaces from microscale to nanoscale will act as the reservoir rocks (Gao et al. 2016; Li et al. 2019; Liu et al. 2020).

Lithology can be identified by core observation, and the discontinuous core can be translated to the continuous petrophysical logs (He et al. 2019; Su et al. 2019). Wireline logs that can be used for lithology identification and prediction include GR, bulk DEN, CNL, AC, resistivity and image logs (Hsieh et al. 2005; He et al. 2019; Nhabanga et al. 2021; Venieri et al. 2021). The organic matter-rich shales and siltstones of Yanchang Formation Member 7 in Ordos Basin have distinct responses on the GR, AC and RT logs (Fig. 8). The black shales recognized on the core have very high GR, high resistivity and high sonic transit time (Venieri et al. 2021) (Fig. 8). For siltstones saturated with oil, the resistivity is also high, but has low GR and low sonic transit time compared with shales (Fig. 8). Additionally, the image logs reveal the internal laminated structure (bedding planes) of shales, while at the siltstone-shale contact surface, a scour surface can be observed (Ran et al. 2016) (Fig. 8). In addition, petrophysical inversion methods can also be used for mineral composition and lithology prediction (Doveton 2014; Ran et al. 2016).

Besides conventional logs, the advanced logs including LithoScanner logs and log processing methods of Quanti elemental log analysis (ELAN) are also useful for lithology identification (Stadtmuller et al. 2018). The prediction of lithology from wireline logs will help extend observations from core scale (centimeters to meters) to the well scale (meters or tens of meters) (He et al. 2019).

4.3 Reservoir Properties and Pore Systems

A series of geological and petrophysical measurements including thin section, scanning electron microscopy (SEM), mercury injection capillary pressure (MICP), nuclear magnetic resonance spectroscopy (NMR) and computed tomography (CT) can be used to characterize the various types of spaces spanning a wide range from nanometer scale to

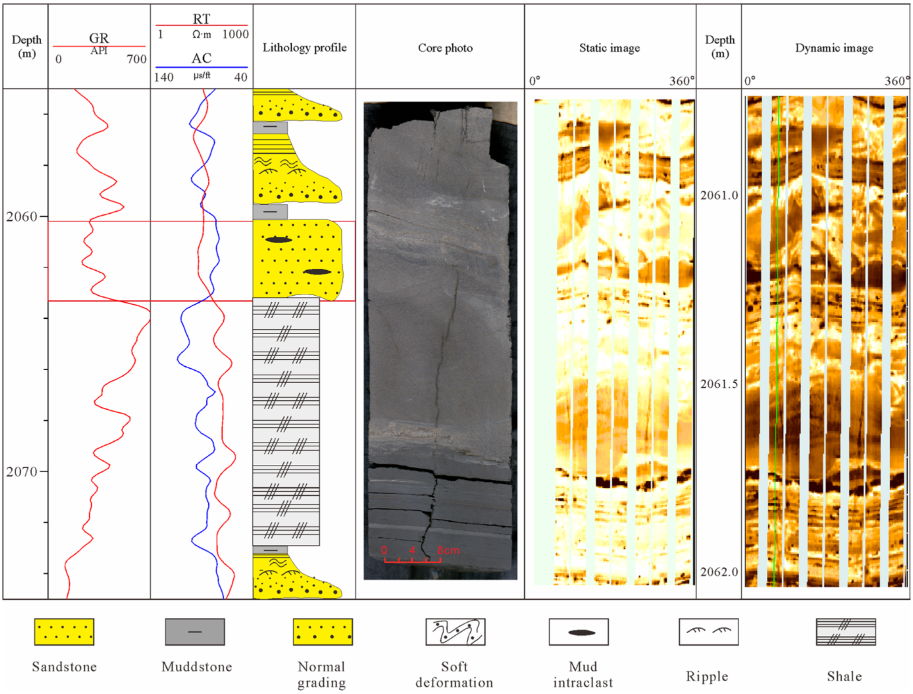

Fig. 8 Well-log expressions of sandstones and shales in Yanchang Formation Member 7 of Ordos Basin, West China

microscales (Josh et al. 2012; Lai et al. 2018b; Zhao et al. 2019; Liu et al. 2019; Du et al. 2021).

In the unconventional hydrocarbon resources, the interbedded siltstone or sandstone as well as carbonate rocks (dolomite, etc.) have anomalously high porosity (Zhao et al. 2019). The siltstone or sandstone intervals contain abundant intergranular pores and intragranular dissolution pores (Fig. 9a, b) (Lai et al. 2018b), while the dolomites (mainly dolomicrite) are dominated by intercrystalline pores as well as intercrystalline dissolution pores (Fig. 9c, d). Fracture and microfracture (aperture < 0.1 mm) also constitute the important reservoir pore spaces in unconventional hydrocarbon reservoirs (Fig. 9e, f).

Shales have ultra-low porosity and the pore spaces (nanopores) are commonly below the resolution of optical microscope (10 μm), but can be easily detected by SEM images (Loucks et al. 2012; Josh et al. 2012; Zhao et al. 2019). The shale reservoirs mainly contain interparticle pores (Fig. 10a), intraparticle pores (Fig. 10b, c), organic matter pores (Fig. 10d) as well as microfractures (Fig. 10e, f) (Loucks et al. 2012; Josh et al. 2012; Su et al. 2018; Chandra and Vishal 2021).

Reservoir quality evaluation using well logs aims at calculating porosity and permeability of the unconventional petroleum reservoir (Schmid et al. 2004). Reservoirs with relatively higher porosity and permeability are called "sweet spots" (Huang et al. 2017). Predicting porosity (including effective porosity), permeability and oil saturation (discussed below) from well-log data is a challenging task because core data are not available for all intervals or wells (Wood 2020b).

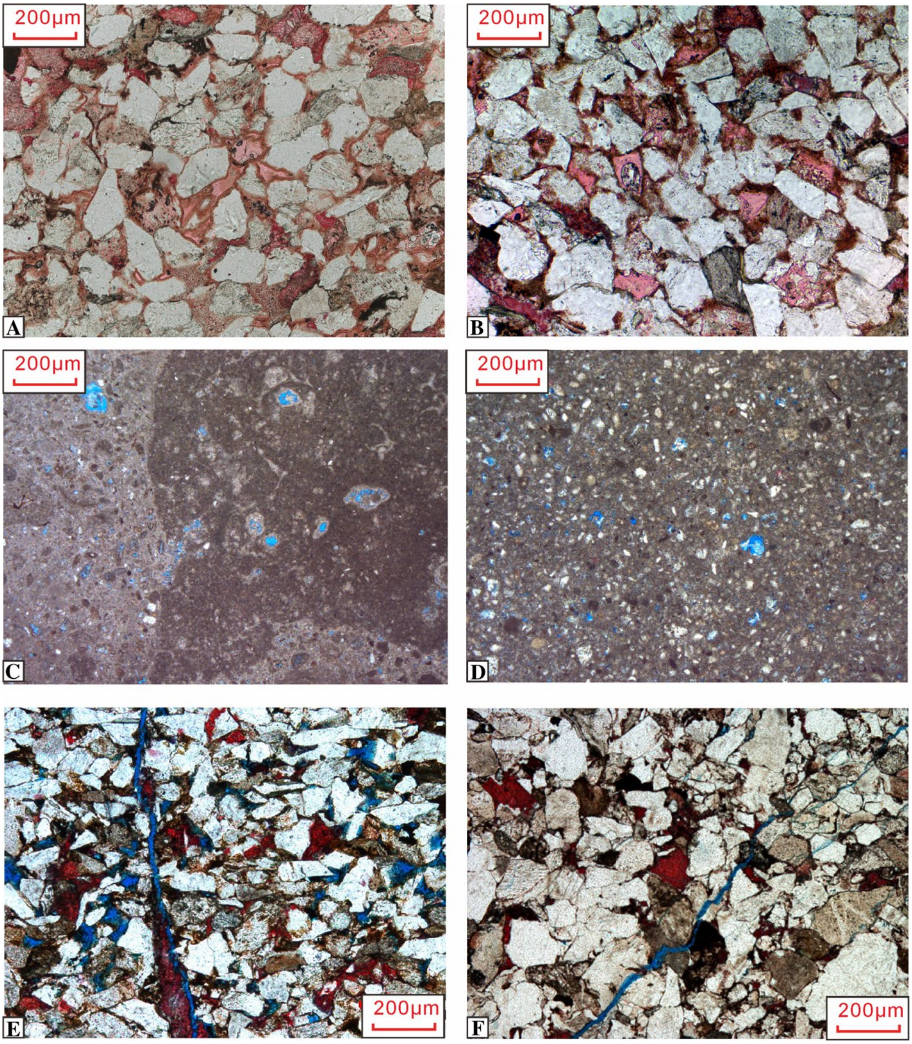

Fig. 9 Thin section images showing the pore spaces of unconventional reservoirs. **a** Intergranular pores in siltstones, Yanchang Formation, Zhuang 234, 1297.07 m, **b** Intragranular dissolution pores in siltstones, Yanchang Formation, Zhuang 233, 1399.32 m, **c** Intercrystal and dissolution pores in dolomicrite, Lucaogou Formation, Ji 174, **d** Intercrystal pores and dissolution pores in dolomicrite, Lucaogou Formation, Ji 174, **e** Microfracture in tight sandstones, DB 14, 6349.34 m, **f** Note that the microfracture is the only pore spaces, DB 17, 6149.24 m

Porosity can be computed using the density log (Iqbal et al. 2018). The effective porosity, which is total porosity without the clay-bound water, can be calculated using the density neutron crossplot method, and also the NMR logs (Stadtmuller et al. 2018). For instance, the ratio of NMR T_2 components > 1.7 ms to the total T_2 components is calculated as effective porosity in Lucaogou Formation in Jimusar Sag of Junggar Basin, and the predicted results are in accordance with the core porosity (Fig. 11) (Wang et al. 2019).

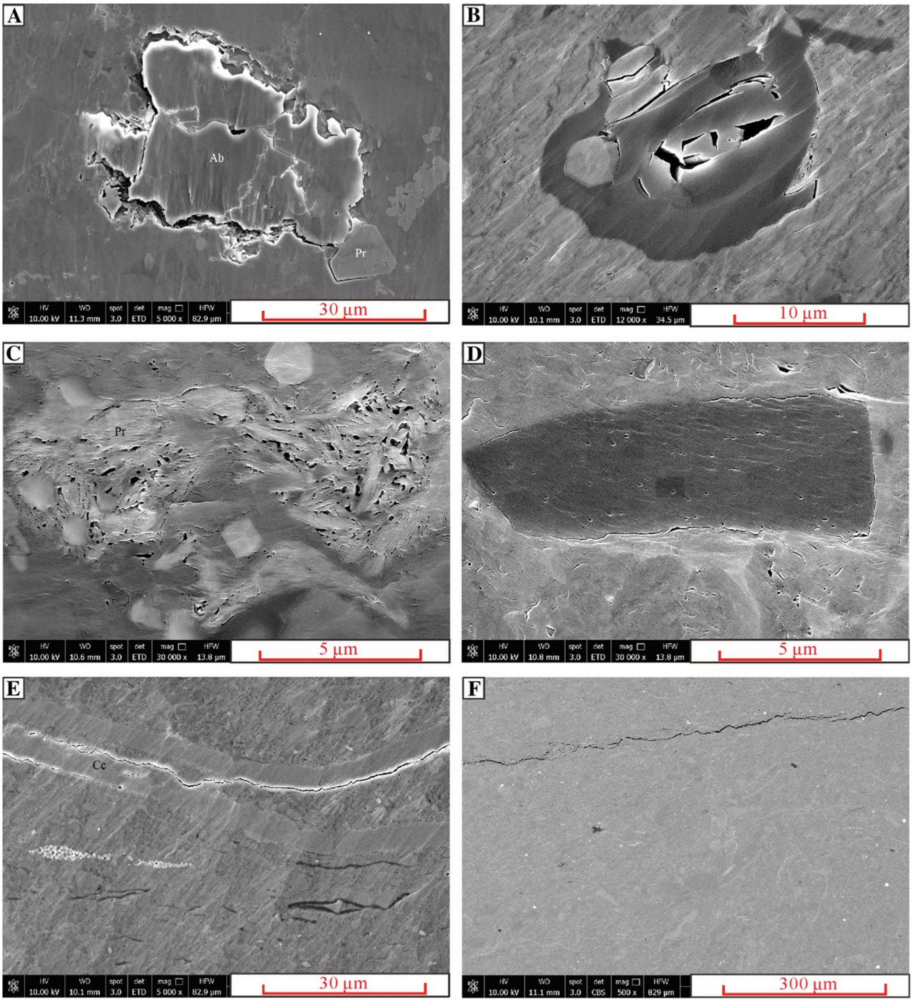

Fig. 10 SEM images showing the pore spaces of oil shale reservoirs. **a** Interparticle pores, **b** Intraparticle pores, **c** Intraparticle pores, **d** Nanopores in organic matters, **e** Microfracture, **f** Microfracture

There are no direct well logs for permeability, but permeability can be derived from NMR logs, and there are two classical model models: the SDR model (Shlumberger Doll research center) (Eq. 4) and the Timur–Coates model (Eq. 5) (Fig. 11) (Coates et al. 1999; Yarmohammadi et al. 2020):

$$K_{\mathrm{SDR}} = D\phi^{4}\left(T_{2\mathrm{gm}}\right)^{2} \tag{4}$$

$$K_{Timu} = \left[\left(\frac{\phi}{C}\right)^{2}\left(\frac{\mathrm{FFI}}{\mathrm{BVI}}\right)\right]^{2} \tag{5}$$

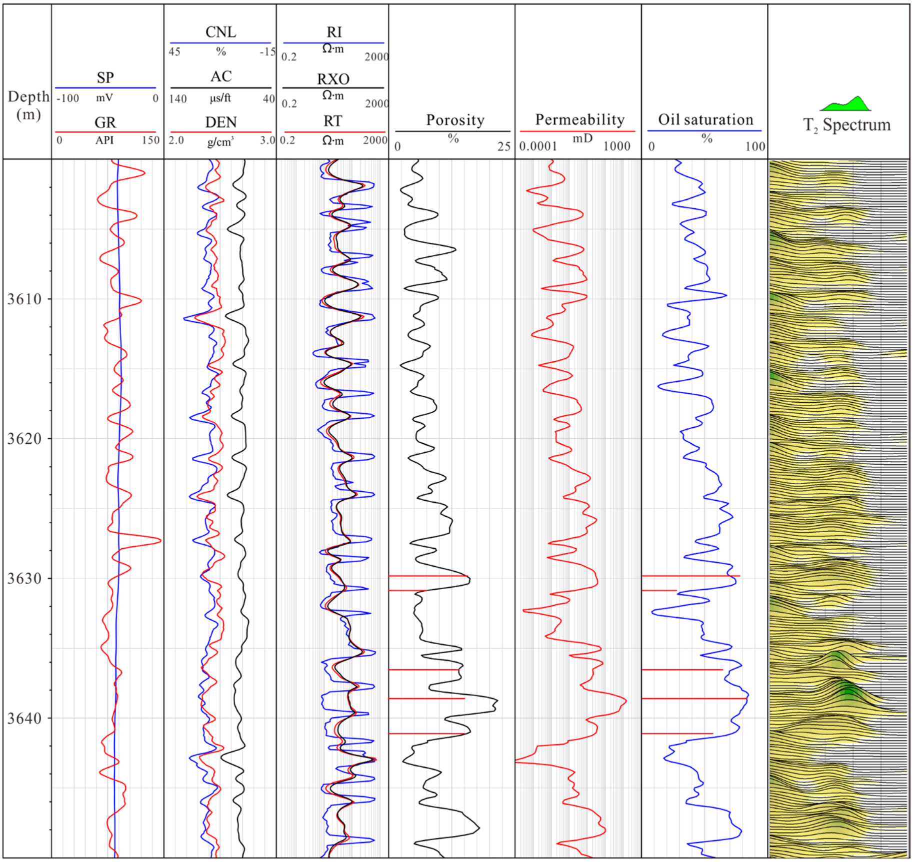

Fig. 11 Calculation of porosity, permeability and oil saturation using NMR log in oil shale reservoirs of Lucaogou Formation in Jimusar Sag, Junggar Basin, West China

K_{SDR} (mD) is permeability from SDR model, and D is a constant (Glover et al. 2006; Rezaee et al. 2012). Where K_{Timu} is permeability in mD, φ is fractional NMR porosity, and FFI free fluid index (FFI) as well as the bulk volume irreducible (BVI). C is also a constant (Rezaee et al. 2012; Yarmohammadi et al. 2020).

Additionally, reservoir quality index (RQI), which was proposed by Amaefule et al. (1993) as the ratio of permeability to porosity under the square root, links the microscopic pore structure with macroscopic reservoir quality (Lai et al. 2016; Henares et al. 2016).

4.4 Oiliness and Oil Bearing Property

Core observation can show the oil bearing grade from low to high grade as fluorescence (no visible oil), oil trace, oil patch, oil immersion, etc. (Wu et al. 2017). Core observation under the fluorescence light will evidently reveal the oil bearing property (Fig. 12). The fluorescence scanning of core shows the varied degree of oil bearing for various

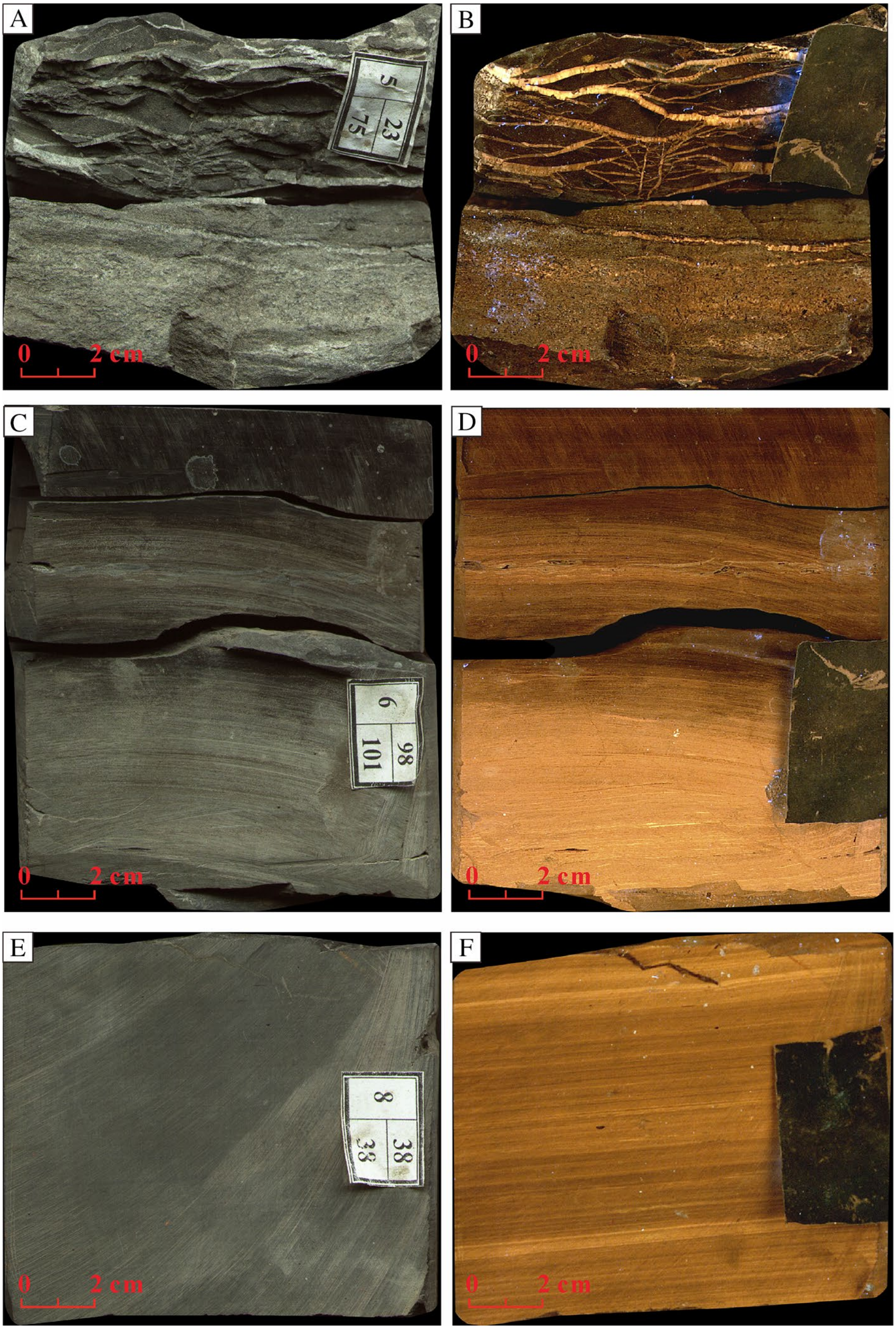

Fig. 12 Core photo taken under the normal and fluorescence light to show the oil bearing property

Fig. 13 Thin section images under plane polarized light and fluorescence light showing the microscopic oil bearing property. **a** Intraparticle dissolution pores, **b** Intraparticle dissolution pores are fluorescent, **c** Microcrystalline dolomite, the dark areas are organic matters, Ji19, 3820.83 m, **d** The dolomite particles are fluorescent, the same field view under fluorescence light of c, **e** Organic matter pores and clay minerals, **f** The organic matter pores and micropores within clays are fluorescent, **g** Filled microfracture, dark organic matters, **h** The microfracture emits blue fluorescence, the same field view under fluorescence light of G

lithologies. The carbonate intervals show strong fluorescence intensity, and the siltstone as well as the dolomite lamina is also fluorescent (Fig. 12).

Interparticle pores are favorable pore spaces for unconventional reservoirs, and almost all the edges of the particles emit strong fluorescences (Fig. 13a, b) (Liu et al. 2020). The intraparticle pores, especially those within carbonate particles, are fluorescent since the carbonate minerals (mainly microcrystalline dolomite) are oil-wet (Fig. 13c, d) (Xi et al. 2019). Organic matter pores as well as micropore associated with clay minerals emit scattered strong blue fluorescence (Fig. 13e, f) (Liu et al. 2020). Microfractures, especially those remain open status, emit strong fluorescences (Fig. 13g–h). The fluorescence thin sections reveal that almost all the entire pore systems in shales are fluorescent (Liu et al. 2021).

Hydrocarbon saturation is also a vital petrophysical parameter, but is difficult to predict via well logs (Zhao et al. 2020). Archie's equation, which is commonly used for fluid saturation calculation, may not be applicable for unconventional reservoirs (Clarkson et al. 2012; Li et al. 2021). The nondestructive NMR log has a distinctive advantage over conventional well logs in unconventional hydrocarbon reservoirs since it can provide petrophysical parameters of porosity, permeability and NMR T_2 amplitude and distribution (Deng et al. 2014; Guo et al. 2020; Li et al. 2020, 2021; Du et al. 2021; Zhang et al. 2021). Therefore, NMR logs are required to provide an accurate estimation of oil saturation (Wang et al. 2020). As is known, hydrocarbon is mainly associated with long T_2 components. Therefore, the NMR T_2 signal amplitudes longer than certain T_2 values (for instance, the threshold value of T_2 is set as 7.0 ms are for Lucaogou Formation in Jimusar Sag) can be treated as hydrocarbon signals, and consequently, the ratio of T_2 components larger than the threshold values to the total effective porosity is calculated as oil saturation (Wang et al. 2019) (Fig. 11). The calculated oil saturation is also in accordance with the core-measured oil saturation (Fig. 11).

4.5 Fracture

Unconventional oil and gas reservoirs (especially shales) have no natural productivity due to their complex pore structure and inherent strong heterogeneity (Zhang et al. 2021). Natural fractures are widespread in unconventional reservoirs (Gale et al. 2014; Lee et al. 2015; Li et al. 2018; Xu et al. 2020). Fractures not only provide pore space for fluid storage, but also greatly improve the reservoir performance, fluid flow, gas enrichment and hydrocarbon productivity (Curtis 2002; Zeng and Li 2009; Zeng et al. 2016; Li et al. 2018; Ladevèze et al. 2018; Basa et al. 2019; Zhang et al. 2021). Additionally, unconventional reservoir relies on hydraulic fracture stimulation (Curtis et al. 2012), and the preexisting (opening-mode) natural fractures will be further reactivated during stimulation and therefore enhance hydrocarbon productivity (Gale et al. 2007, 2014).

The fracture effectiveness of fracture is determined by the attitudes of fractures (high-angle, low-angle, horizontal and network fractures), scale of fractures (macroscopic and microfractures) and status fracture surface (open and closed fracture) (Gale et al. 2014;

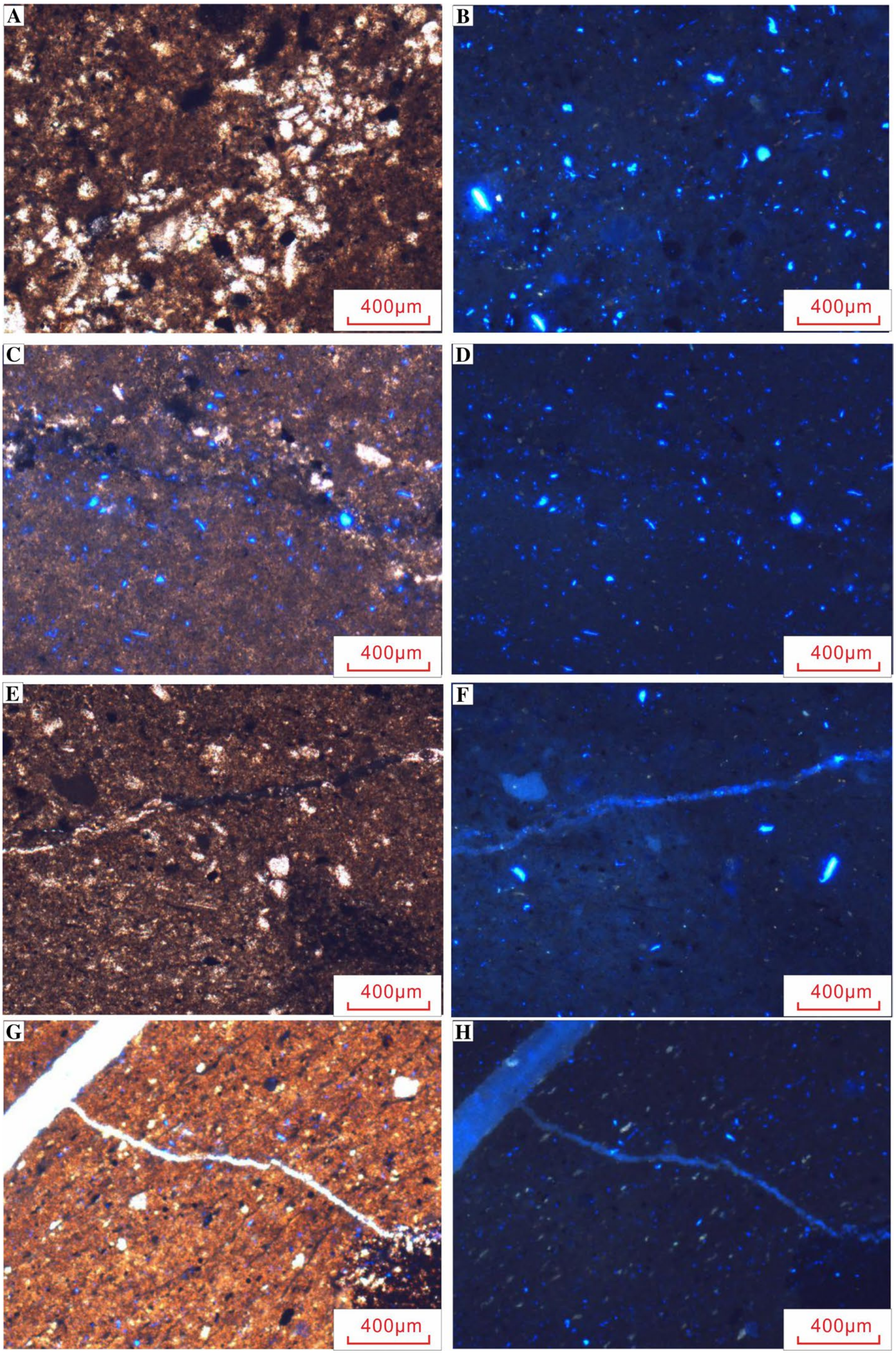
A
400μm
B
400μm
C
400μm
D
400μm
E
400μm
F
400μm
G
400μm
H
400μm

Hooker et al. 2017; Zhang et al. 2021). Consequently, the prediction and evaluation of subsurface fracture are important for unconventional hydrocarbon reservoir assessment (McGinnis et al. 2017; Lai et al. 2018a; Ladevèze et al. 2018).

Borehole image logs, which have a vertical resolution of 5 mm, are sensitive for the rock composition, structure and fluids in the formation (Ameen 2014; Zhang Shaolong et al. 2021). The presence of natural fractures will cause a rapid decrease in resistivity, and the fracture planes will appear as a sinusoidal wave on the image logs (Lai et al. 2021). Fractures in the Xujiahe Formation Member 2 of Sichuan Basin have caused rapid decrease in resistivity (Fig. 14). The fracture attitudes (dip and dip angles), fracture status (open, sealed, partly sealed) and fracture parameters (fracture length, aperture, porosity and density) can be picked out from the sinusoidal curves on image logs (Fig. 14) (Lai et al. 2019). Fractures can be divided into conductive and resistive types, and interpreted as partially or fully open and sealed fractures in terms of image log interpretation (Hooker et al. 2017). High-angle fractures will trace as sinusoids, whereas the planar or horizontal fractures intersect the circular wellbore (Fig. 14) (Hooker et al. 2017).

The conventional well-log suits sensitive for the natural fractures include deep and shallow resistivity logs (Rt, Rxo), CAL as well as three porosity logs, especially AC, are sensitive for the presences of natural fractures (Khoshbakht et al. 2012; Zazoun 2013;

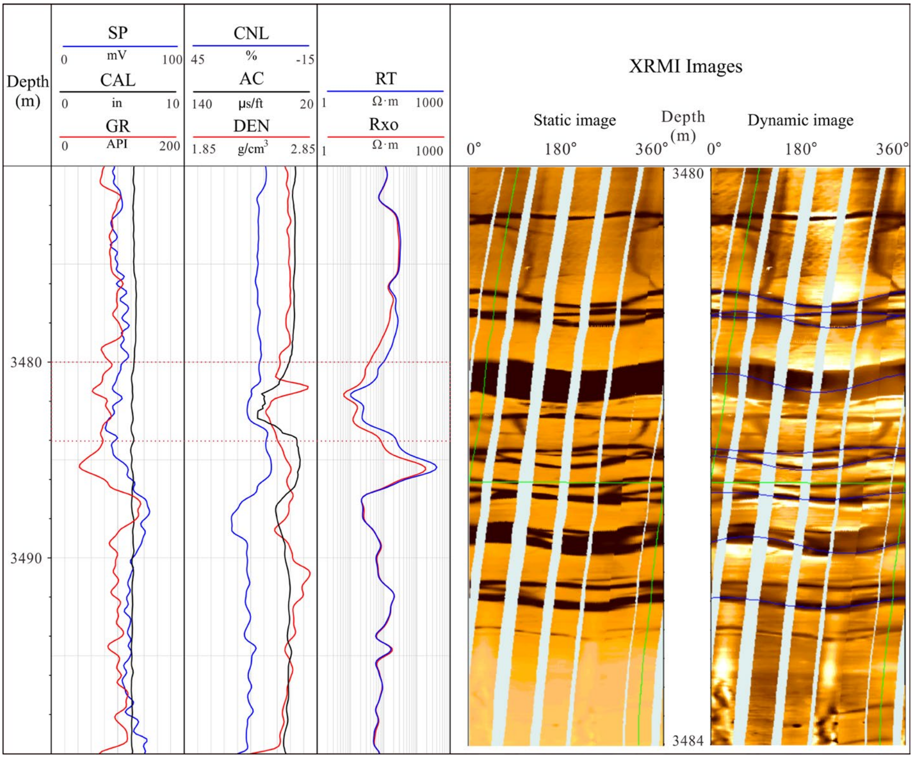

Fig. 14 Fracture responses on conventional and image logs in tight gas sandstones (Xujiahe Formation Member 2 of Sichuan Basin, West China)

Aghli et al. 2016; Lai et al. 2021). There is an evident decrease in lateral resistivity logs and density logs, while the AC values are significantly increased in the fractured intervals (Fig. 14).

Bed-parallel (horizontal) fractures are more prevalent in unconventional reservoirs (primarily fine-grained sedimentary rocks) than in sandstone or carbonate rocks (Fig. 15) (Gale et al. 2014). Layered structures are common in the fine-grained sedimentary rocks, which act as reservoirs for unconventional resources (Gale et al. 2014; Yawar and Schieber 2017). The multiple lamina or weak bedding interfaces, which are easily opened due to changing of in situ stress status, are favorable for formation of bedding parallel fractures (Zhang et al. 2017a, b). These bedding parallel fractures, which occur as horizontal fractures (Fig. 15), strongly influence fluid flow, and therefore hydrocarbon storage and productivity (McGinnis et al. 2017; Basa et al. 2019; Liang et al. 2021).

The bedding parallel fractures in Yanchang Formation Member 7 of Ordos Basin result in the reduction of resistivity and bulk density, but the sonic transit time increases (Fig. 15). Besides conventional logs and image logs, sonic scanner logs are also sensitive for the fractures (Zaree et al. 2016). The sonic transit time will increase, and the amplitudes of full wave forms will be attenuated, showing V-shape interferometric fringe in the

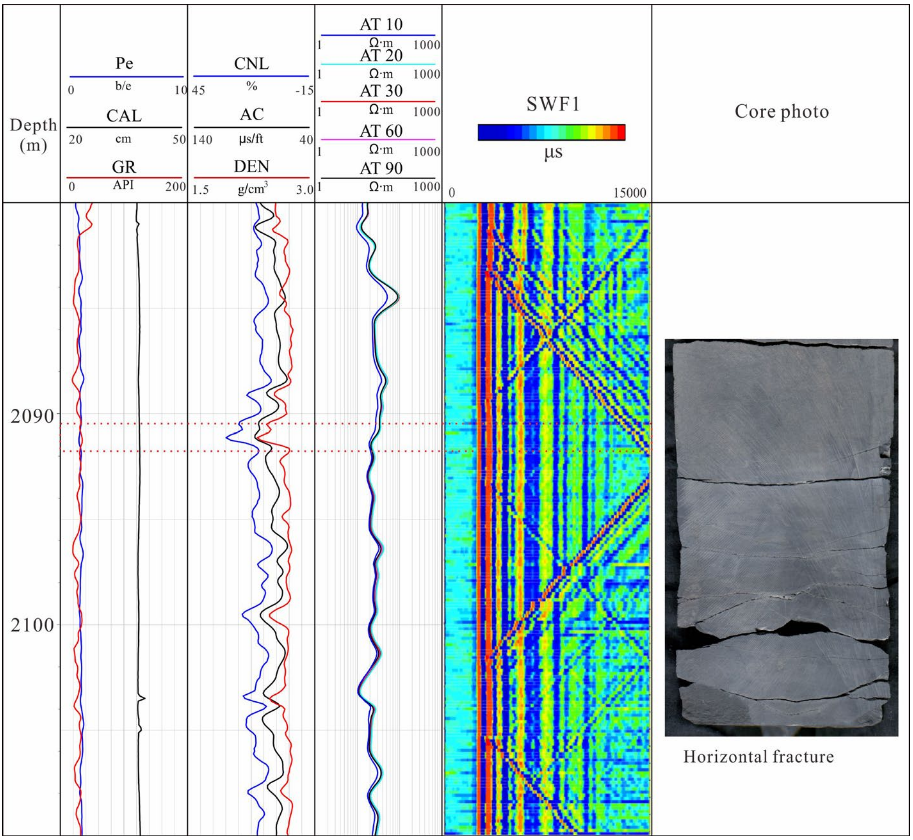

Fig. 15 Well-log responses of horizontal fractures in shale oil reservoirs (Yanchang Formation Member 7 of Ordos Basin, West China)

fractured zones (Collett et al. 2011; Assousa and Elkington 2014; Zaree et al. 2016; Lai et al. 2017) (Fig. 15).

5 Engineering Property

Horizontal well drilling and multi-stage hydraulic (volume) fracturing are required for efficient exploitation of unconventional hydrocarbon resources due to their ultra-low matrix permeability (Curtis et al. 2012; Clarkson 2013; Fuentes-Cruz et al. 2014; Avanzini et al. 2016; Dong et al. 2018; Liu 2021). The implementation of advanced drilling and completion techniques significantly improve the successful production of hydrocarbons (Curtis et al. 2012; Clarkson 2013). Engineering property evaluates the brittleness, fracability, in situ stress anisotropy and magnitudes for unconventional hydrocarbon resources (Rybacki et al. 2016; Avanzini et al. 2016; Iqbal et al. 2018; Zhao et al. 2019; Yarmohammadi et al. 2020). Therefore, brittleness and in situ stress states and magnitudes are critical parameters for optimizing engineering sweet spots during hydraulic fracturing in unconventional reservoirs (Gale et al. 2007; Iqbal et al. 2018).

Brittleness evaluates the rock behavior of fracability during hydraulic fracturing (Verma et al. 2016; Iqbal et al. 2018). Brittle layers are easier to form fracture network than ductile layers (Soliman and Kabir 2012; Iqbal et al. 2018; Sun et al. 2021). The present-day maximum horizontal stress controls the geometry of the natural fracture system and direction of hydraulic fracture propagation, and therefore is important for design of hydraulic fracture treatment (Gale et al. 2007). Therefore, engineering property evaluation mainly focuses on the brittleness index and in situ stress fields (Avanzini et al. 2016; Iqbal et al. 2018).

5.1 Brittleness Index

Brittle layers with high brittleness index, which are easier to be fractured (brittle enough to initiate fractures), and to keep the fractures open, will be optimized for hydraulic fracturing in unconventional resources (Rickman et al. 2008; Sondergeld et al. 2010; Josh et al. 2012; Lai et al. 2015; Gholami et al. 2016; Iqbal et al. 2018; Nhabanga et al. 2021). In terms of geomechanical evaluation, brittleness is closely associated with elastic parameters Young's modulus (E) and Poisson's ratio (v) (Iqbal et al. 2018; Mews et al. 2019). Poisson's ratio is the ratio of transverse to axial strain, and measures the rock's ability to form fractures under stress. Young's modulus is a ratio of stress to strain, and measures the rock's ability to maintain fracture after treatment (Iqbal et al. 2018). Ductile rock may require more energy/fracturing pressure to break, and fractures formed by hydraulic fracturing in ductile rocks may easily be healed (Iqbal et al. 2018).

From a petrophysical point of view, there are two commonly used methods to calculate brittleness index. The first is the brittle mineral content, while the second is the elastic rock parameters (Young's modulus and Poisson's ratio) (Guo et al. 2015; Lai et al. 2015; Fan et al. 2019; Zhao et al. 2019; Wood 2021).

The brittleness index (%) derived from Young's modulus and Poisson's ratio can be defined as the average of the BI_E and BI_ν (Eqs. 6–8) (Lai et al. 2015; Iqbal et al. 2018; Fan et al. 2019). Brittle rocks have higher Young's modulus and lower Poisson's ratio (Rybacki et al. 2016; Zhang et al. 2016; Iqbal et al. 2018; Kumar et al. 2018). High Young's modulus is associated with layers of low porosities but high brittle minerals (quartz, carbonate and feldspar) (Liu et al. 2018).

$$BI = \frac{BI_E + BI_v}{2} \times 100\% \tag{6}$$

$$BI_E = \frac{E - E_{min}}{E_{max} - E_{min}} \tag{7}$$

$$BI_v = \frac{v - v_{max}}{v_{min} - v_{max}} \tag{8}$$

where E (GPa) is Young's modulus and v (dimensionless) is Poisson's ratio. v_{min} and v_{max} are the minimum and maximum Poisson's ratio, whereas E_{min} and E_{max} are the minimum and maximum Young's modulus.

The dynamic Young's modulus and Poisson's ratio can be calculated from V_p, V_s and bulk density logs (Eqs. 9–10) (Lai et al. 2015).

$$E = \frac{\rho}{V_s^2} \frac{3V_p^2 - 4V_s^2}{V_p^2 - V_s^2} \tag{9}$$

$$v = \frac{V_p^2 - 2V_s^2}{2(V_p^2 - V_s^2)} \tag{10}$$

where ρ is the bulk density log (kg/m^3), while V_p is the P (compressive) wave velocity (m/s), and V_s is S (shear) wave velocity (m/s) (Lai et al. 2015).

Dynamic Young's modulus and Poisson's ratio calculated using sonic and density logs should be calibrated with the static elastic parameters (core-measured) to improve accuracy (Iqbal et al. 2018).

Jarvie et al. (2007) defined the mass ratio of quartz to all minerals as index of brittleness. However, besides quartz, the carbonates are also brittle minerals (Jarvie et al. 2007; Rybacki et al. 2016; Fan et al. 2019; Qian et al. 2020).

The method to calculate brittleness index using brittle mineral content is written as (Eq. 11).

$$BI = (Qz + Car)/(Qz + Car + Fels + Clay) \times 100\% \tag{11}$$

Qz is quartz content, %, Car is the carbonate content, %, Fels is the feldspar content, %, and Clay is the total clay content by weight, %. Rocks with brittleness index > 40% are treated as brittle rocks (Guo et al. 2015; Lai et al. 2015; Iqbal et al. 2018).

The elastic parameters (v and E) can be calculated from the well logs of V_p, V_s and density logs. Then, the Poisson's ratio–Young's modulus method can be adapted to calculate brittleness index (Kumar et al. 2018). Layers with low Poisson's ratio and high Young's modulus contribute to a high brittleness index, and they are favorable for hydraulic

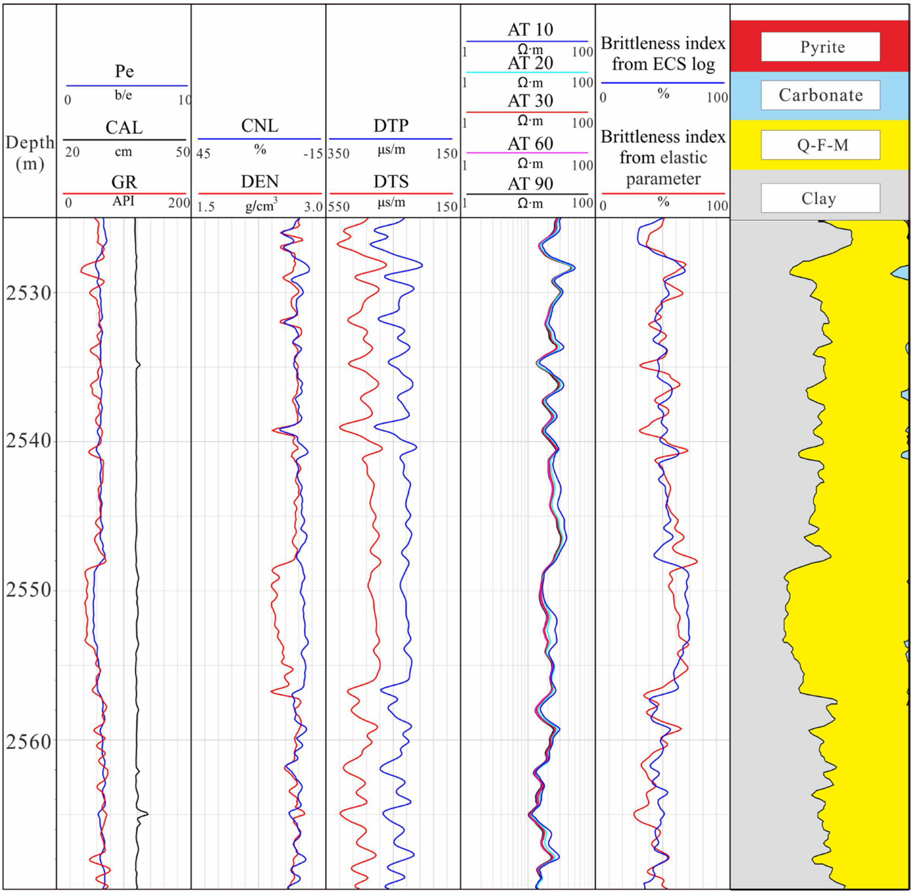

Fig. 16 Comparison of brittleness index calculated by Young's modulus–Poisson's method and by ECS logs

fracturing, and maintaining as well as propagating fractures (Fig. 16) (Rybacki et al. 2015; Kumar et al. 2018).

Additionally, the ECS logs, which can derive the rock compositions of clay, Q–F–M (quartz, feldspar and mica), carbonate, etc., can be used to calculate the brittleness index using the method of brittle mineral ratio (Fig. 16) (Maliva et al. 2009; Lai et al. 2015; Kumar et al. 2018). The brittleness index calculated by the two methods (mineralogy method and elastic parameter method) is generally in accordance with each other (Fig. 16).

5.2 In Situ Stress Status and Direction

The in situ stress fields commonly include vertical stress (S_v), direction and magnitudes of maximum horizontal stress (SH_{max}) and minimum horizontal stress (Sh_{min}), as well as formation pressure (P_p) (Zoback et al. 2003; Verweij et al. 2016; Dixit et al. 2017; Lai et al. 2019).

Besides brittleness index, in situ stress fields also play critical roles in hydraulic fracturing and horizontal well trajectory design (Qian et al. 2020). For engineering "sweet spot" evaluation, brittleness measures the ability to form fracture and keep fracture open, while the in situ stress field (direction and magnitude) evaluates the horizontal well trajectory design and propagation of hydraulic fractures (Josh et al. 2012). A large amount of high-pressure fluids are injected into the formation to reopen the natural fracture system and create new hydraulic fractures during hydraulic fracturing (Rybacki et al. 2016; Zhao et al. 2019). Consequently, a complex and new pore–fracture network system will be formed and hydrocarbon will migrate toward the wellbore for production (Zhao et al. 2019).

Therefore, the magnitude and direction of in situ stresses are also required to optimize the prospected layers for hydraulic fracturing (Josh et al. 2012; Iqbal et al. 2018). The direction of in situ stress fields determines the drilling direction of horizontal wells, and the propagation of hydraulic fractures. Brittleness alone is not sufficient to optimize prospected layers, and the magnitudes of in situ stress are also an important index for optimizing prospected layers for engineering sweet spots. Complex and new pore–fracture systems will be formed in layers with low horizontal stress differences.

5.2.1 Direction of In Situ Stress

The brittleness affects the formation and preservation of natural fractures, while the in situ stress fields control the initiation and propagation of hydraulic fractures (Fig. 17) (Josh et al. 2012; Rybacki et al. 2016). Brittle rocks are expected to contain more natural

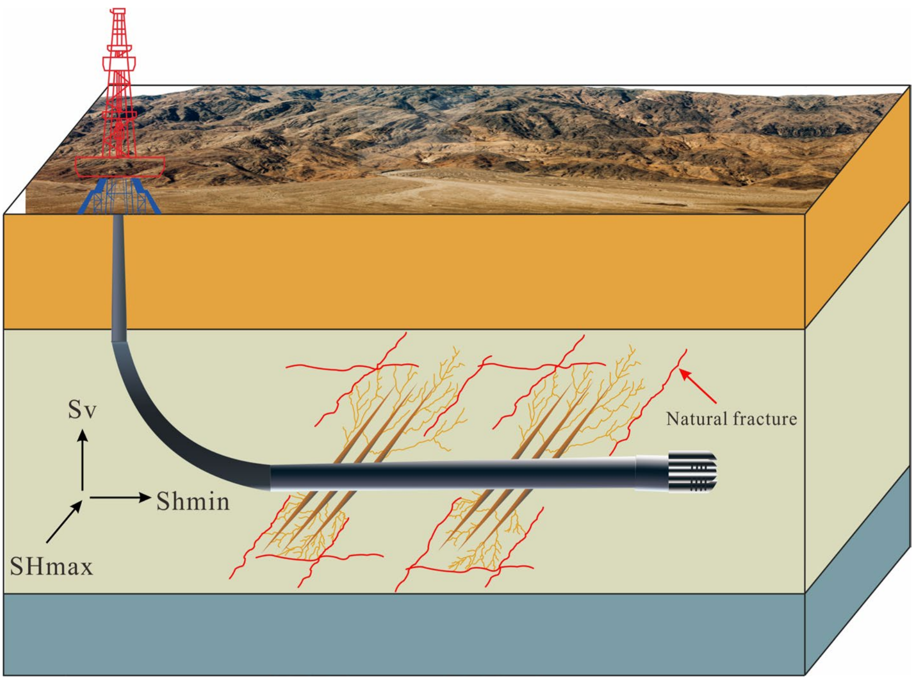

Fig. 17 Horizontal drilling direction, hydraulic fracture propagation and in situ stress field in unconventional hydrocarbon resources

fractures and are more easily to be fractured by hydraulic stimulation (Gale et al. 2007; Rybacki et al. 2016; Zhang et al. 2016). In addition, the hydraulic fractures will propagate along the direction of maximum horizontal stress (SH_{max}) (Kingdon et al. 2016; Iqbal et al. 2018). Hydraulic fractures follow SH_{max}, until they encounter the preexisting natural fractures, and then, the hydraulic fractures will be blocked from further propagation (Gale et al. 2007). Consequently, the horizontal wells are drilled along the minimum horizontal stress (Sh_{min}), and hydraulic stimulation will be toward the SH_{max} direction (Josh et al. 2012; Iqbal et al. 2018). In this situation, a large number of hydraulic fractures will be formed along the SH_{max} direction, and these induced fractures will intersect with the preexisting fractures to form complex fracture networks (Fig. 17).

Image logs, which can pick out the borehole breakouts and induced fractures, are widely used for the determination of SH_{max} and Sh_{min} (Lai et al. 2018a; Stadtmuller et al. 2018). The borehole breakouts, which appear as broad, parallel, dark bands with 180° apart on image logs, indicate the orientations of Sh_{min} (Massiot et al. 2015; Nian et al. 2016) (Fig. 18a). The drilling induced fractures are recognized as two vertical fractures ("two ways") with 180° offset at the borehole surfaces on the image logs (Fig. 18b), and they show the orientations of SH_{max} (Ameen et al. 2012; Khair et al. 2013; Nian et al. 2016; Lai et al. 2019). Consequently, both the induced fractures and borehole breakouts can unravel the in situ orientation. Natural fractures can be distinguished from drilling induced fractures and borehole breakouts on image logs by their continuous sinusoid nature (Fig. 14) (Khair et al. 2015).

Besides image logs, the sonic logs, which provide the shear-wave velocities and direction, can reveal the in situ stress fields (Stadtmuller et al. 2018). As is known, in anisotropic rocks, the shear wave will be split into fast and slow waves, i.e., shear-wave birefringence (Liu et al. 2018). Therefore, fast S-wave azimuth indicates the SH_{max} direction (Liu et al. 2018; Stadtmuller et al. 2018) (Fig. 19). The SH_{max} direction can be determined from the fast S-wave azimuth as near NW–SE to S–E direction (Fig. 19).

5.2.2 In Situ Stress Magnitudes

In situ stress magnitudes play vital roles in different aspects of hydraulic fracturing treatment (Iqbal et al. 2018). The difference between SH_{max} and Sh_{min} (SH_{max}–Sh_{min}) is important for directional drilling, hydraulic fracturing design, and optimization of engineering "sweet spots" (Stadtmuller et al. 2018). Intervals with low differences between SH_{max} and Sh_{min} are suggested to be easily fractured and therefore will be optimized for hydraulic fracturing.

The vertical stress (Sv) is commonly calculated by integrating the weight of the overburden rocks by well logs (Eq. 12) (Fig. 20) (Maleki et al. 2014; Verweij et al. 2016; Iqbal et al. 2018; Lai et al. 2022).

$$S_v = \int_0^Z \rho g dz \tag{12}$$

In this formula, Z is the burial depth, m, g is the gravitational acceleration (m/s^2), and ρ is the bulk density, kg/m^3 (Maleki et al. 2014; Verweij et al. 2016).

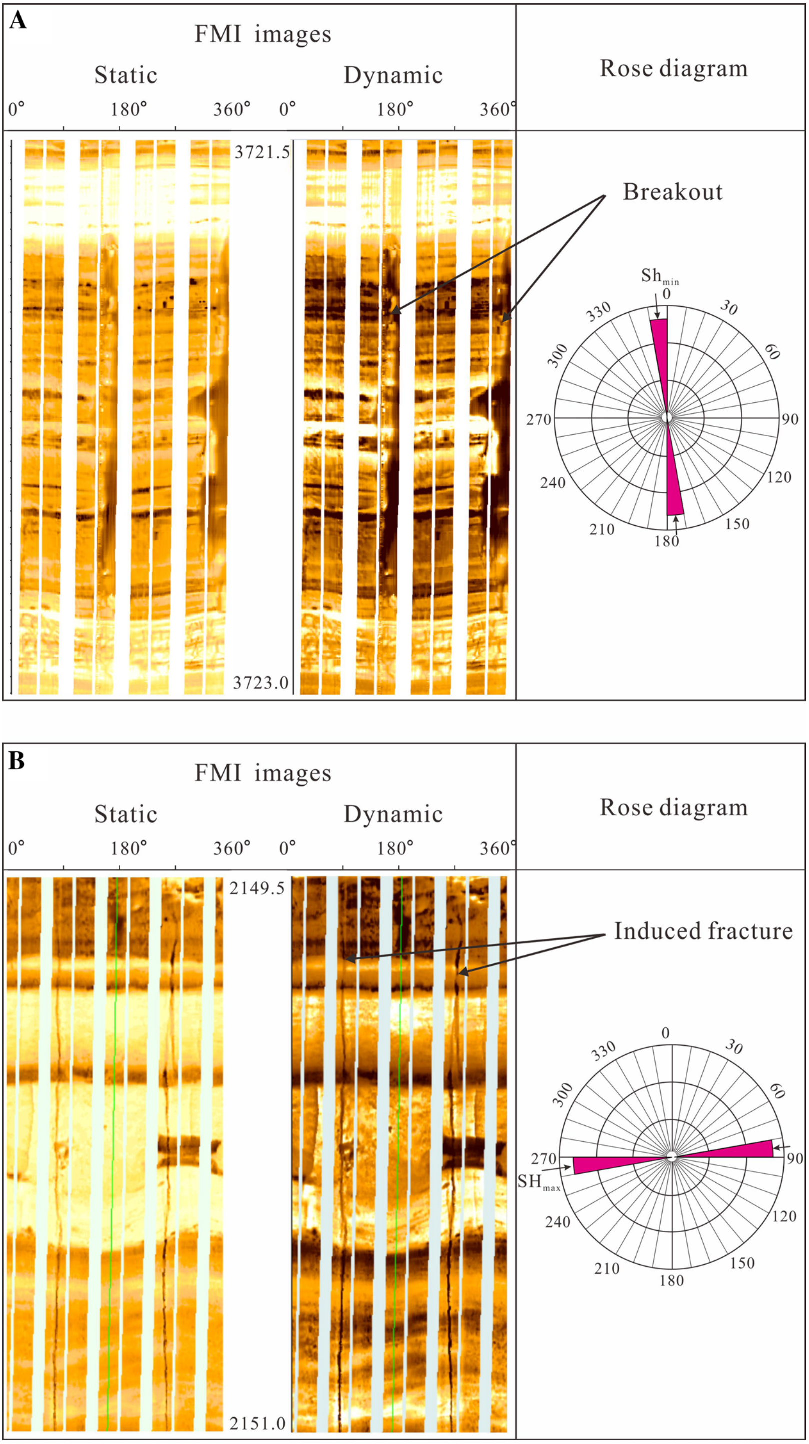

Fig. 18 In situ stress direction determined from image logs

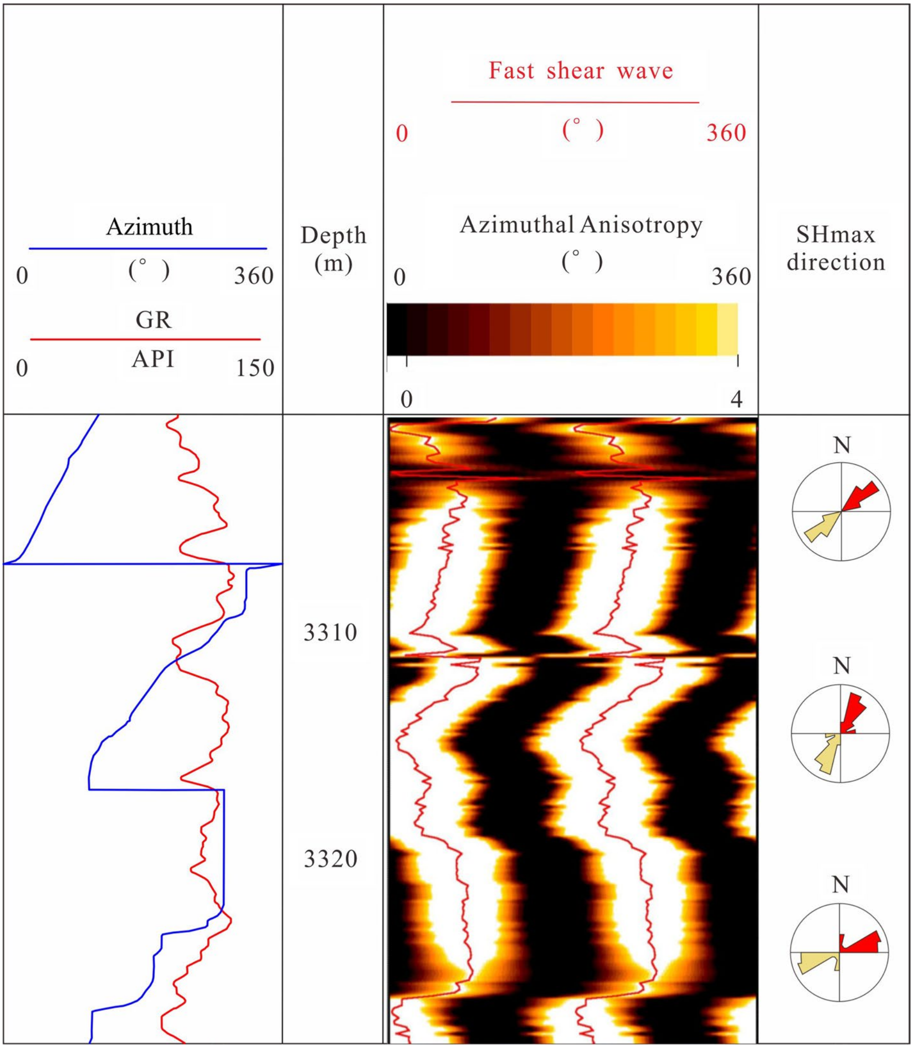

Fig. 19 Maximum horizontal stress (SHmax) direction from sonic fast shear-wave orientation

The two components of horizontal stress (SH_{max}, Sh_{min}) are closely associated with elastic modulus (Young's modulus and Poisson's ratio) (Du et al. 2021). The one-dimensional mechanical earth model is commonly adopted to calculate the horizontal stresses using poroelastic theory (Eqs. 13, 14) (Fig. 20) (Engelder 1993; Zoback et al. 2003; Stadtmuller et al. 2018; Lai et al. 2022).

$$SH_{max} = \frac{\nu}{1-\nu}(Sv - \alpha P_p) + \alpha P_p + \frac{E\varepsilon}{1-\nu^2} \tag{13}$$

$$Sh_{min} = \frac{\nu}{1-\nu}(Sv - \alpha P_p) + \alpha P_p + \frac{E\nu\varepsilon}{1-\nu^2} \tag{14}$$

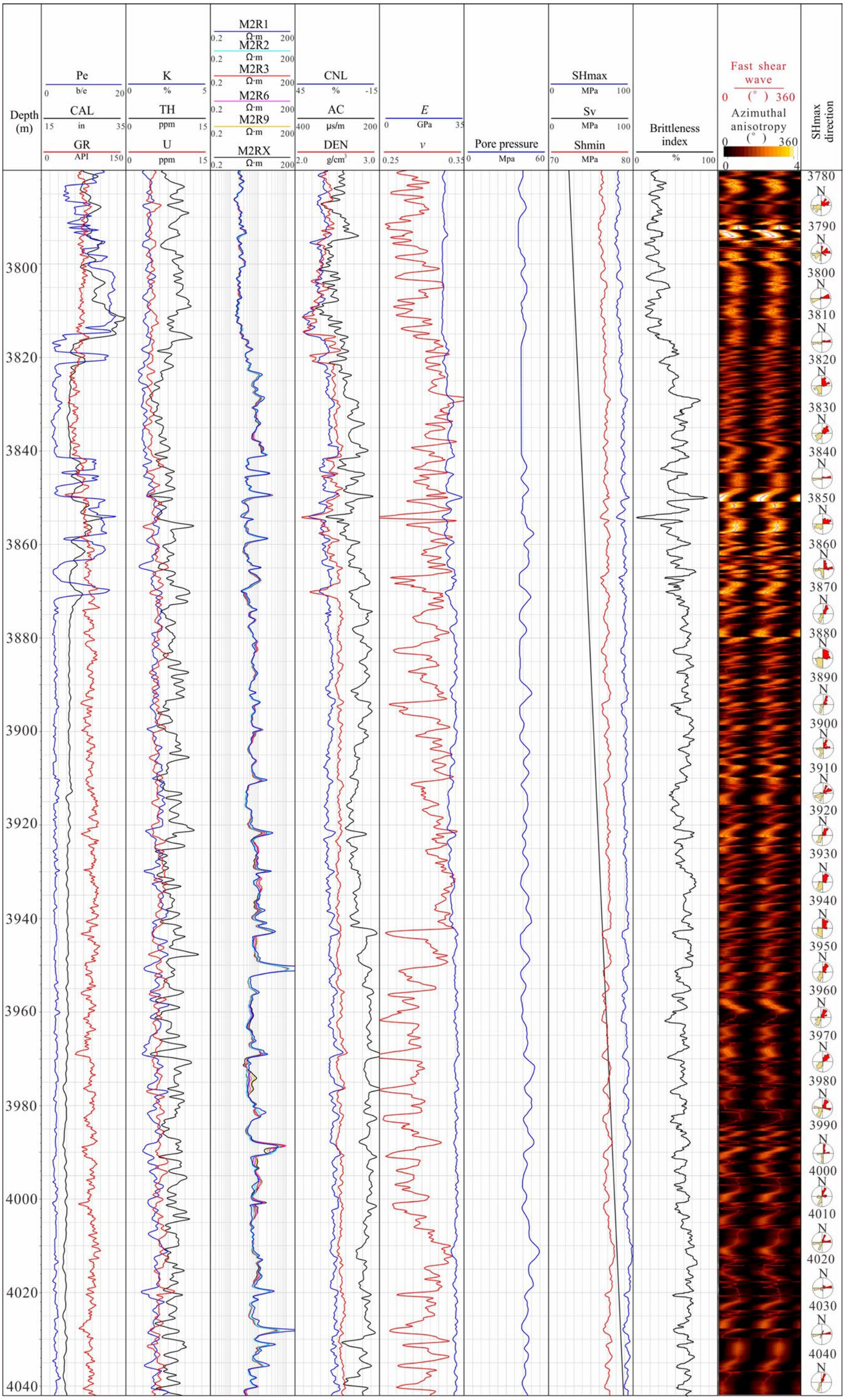

Fig. 20 The in situ stress fields (direction and magnitudes) and brittleness index calculated from well logs

In Eqs. (13) and (14), α is the Biot's coefficient. P_p is pore pressure, and can be derived from the Eaton's method. The ε is strain factor (Stadtmuller et al. 2018; Iqbal et al. 2018). Consequently, the horizontal stresses can be calculated from Sv, E, v, Biot's coefficient, strain factor and pore pressure (Iqbal et al. 2018).

The tectonic regimes proposed by Anderson (1951) can be determined from the relative amplitudes of the three stress components, and they include normal ($Sv > SH_{max} > Sh_{min}$), strike-slip ($SH_{max} > Sv > Sh_{min}$) and thrust faulting stress regime ($SH_{max} > Sh_{min} > Sv$) (Zoback et al. 2003; Verweij et al. 2016; Dixit et al. 2017; Stadtmuller et al. 2018; Lai et al. 2019). The strike-slip faulting stress regime is encountered in Fig. 20 (Lai et al. 2022).

Engineering property evaluation should comprehensively take brittleness index as well as in situ stress direction and magnitude into consideration. The horizontal wells are designed to drill parallel to Shmin, with the aim to maximize the volume stimulated by induced fractures (Gale et al. 2007). The dominant SH_{max} direction (fast shear wave) is NE–SW direction (Fig. 20) (Lai et al. 2022). Then, the layers with high brittleness index but low horizontal principle stress differences will be optimized for hydraulic fracturing in order to create the most abundant hydraulic fracture networks (Stadtmuller et al. 2018).

6 Optimization of Sweet Spots

Unconventional hydrocarbon resources have no natural productivity; therefore, the identification of sweet spots is important (Zou et al. 2019). Sweet spots in unconventional resources refer to the best zones or intervals for hydrocarbon exploration and exploitation, and there are mainly geological and engineering sweet spots (Lu et al. 2019; Zhao et al. 2019; Zou et al. 2019). Geological sweet spots are the zone or intervals with the best reservoir quality and oil bearing property, and they can be optimized considering reservoir property (lithology, porosity, oil saturation), and presence of natural fractures (Zhao et al. 2019; Zou et al. 2019). Engineering sweet spots refer to the zone or intervals prospected for hydraulic fracturing stimulation, and therefore, brittleness and in situ stress anisotropy are the critical parameters to be evaluated (Rybacki et al. 2016; Iqbal et al. 2018; Zhao et al. 2019).

Insights into the seven kinds of parameters (lithology, reservoir quality, hydrocarbon bearing property, well-log responses, source rock property, brittleness and in situ stress field) and three types of properties (source rock property, reservoir property and engineering property) lay the foundation for sweet spot optimization using well logs (Zou et al. 2019). Geological sweet spot evaluation aims at selecting the favorable hydrocarbon bearing reservoirs; therefore, the lithology, porosity, hydrocarbon saturation, fracture and source–reservoir assemblage should be evaluated. Engineering sweet spot evaluation focuses on optimizing the prospected layers for hydraulic stimulation, and therefore, evaluation of geomechanical property (brittleness index, in situ stress) is particularly important (Zhang et al. 2017a, b; Iqbal et al. 2018; Zhao et al. 2019). Both the petrophysical attributes and geomechanical properties need to be fully understood to identify the prospected sweet spots (Iqbal et al. 2018).

6.1 Relationships Between the Three Types of Properties

Relationships between the source rock property, reservoir property and engineering property should be unraveled when selecting the prospected layers for production. TOC is an excellent indicator of organic matrix and hydrocarbon potential as well as source rock property, and TOC can be continuously evaluated via well logs (Amosu et al. 2021). Reservoir property in terms of porosity, permeability and oil saturation can be predicted by integrating conventional logs and NMR log (Wang et al. 2019). Brittleness and in situ stresses, which describe the engineering property, can be estimated according to the elastic parameters using sonic logs (Iqbal et al. 2018; Zhao et al. 2019).

Source rock intervals in Funing Formation in Subei Basin (East China), which have high TOC content, have low reservoir property as can be observed from the crossplot of porosity versus TOC content (Fig. 21). In addition, TOC shows negative correlation relationships with horizontal stress difference (SH_{max}–Sh_{min}) (Fig. 22a), indicating that source rock intervals can also be fractured due to the low horizontal stress differences. The brittleness index shows complex relationship with TOC and rocks with brittleness index 40–60% have the highest TOC values, indicating brittleness is complex reflection of lithology, composition, TOC and diagenesis (Clarkson et al. 2012; Iqbal et al. 2018) (Fig. 22b).

Petrophysical properties affect the geomechanical properties of unconventional reservoirs (Iqbal et al. 2018; Zhao et al. 2019). Engineering property shows complex relationships with reservoir property as can be indicated by the crossplots of brittleness index and horizontal stress difference with porosity (Fig. 23a, b). Therefore, the reservoir property, which describes the geological sweet spots, is not matching the engineering property characterizing the engineering sweet spots (Fig. 23).

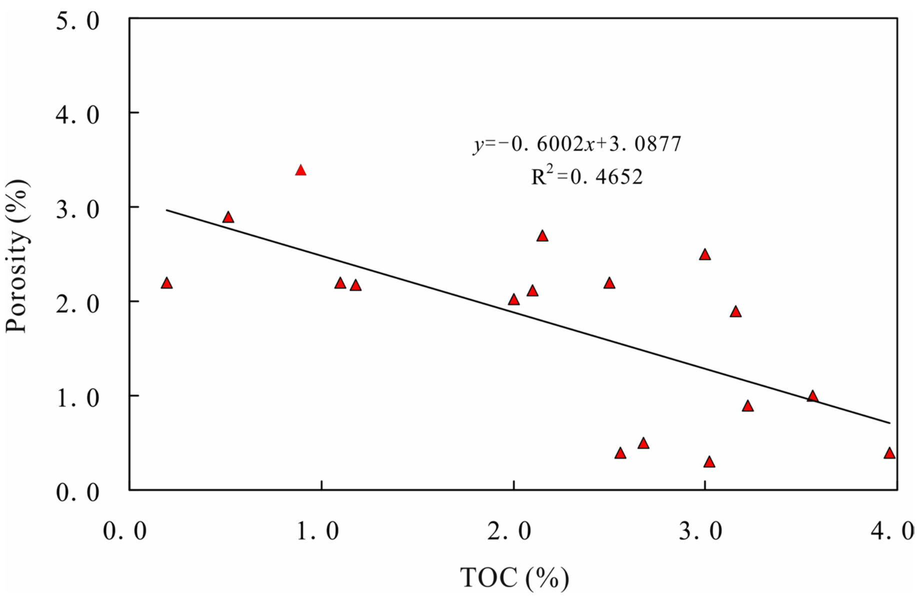

Fig. 21 Crossplot of porosity versus TOC of Funing Formation in Subei Basin, East China

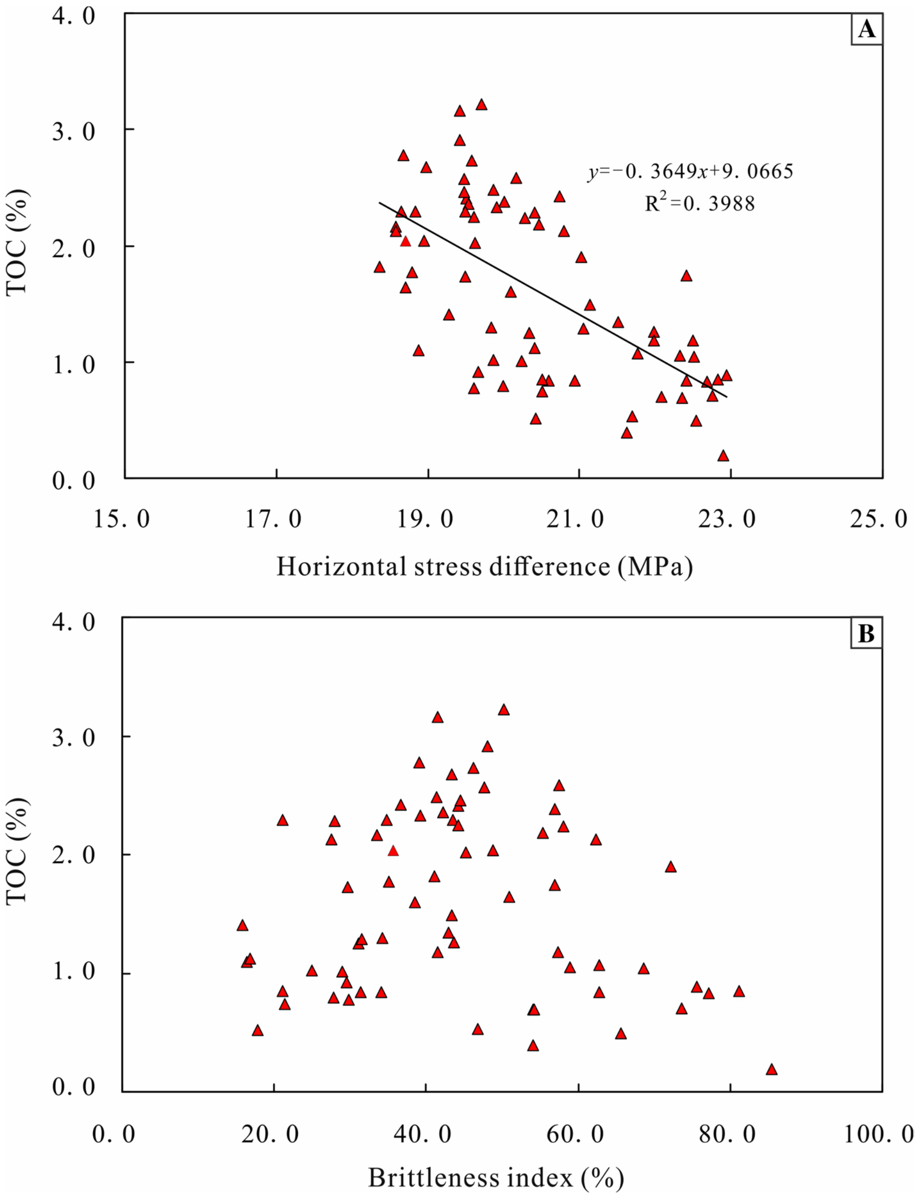

Fig. 22 Crossplots of TOC versus horizontal stress difference and brittleness index in Funing Formation in Subei Basin, East China

6.2 Optimization of Geological and Engineering Sweet Spots

The three types of properties determine the distribution of sweet spots (Zhao et al. 2019). The source rock property is evaluated in terms of TOC content as well as the conventional

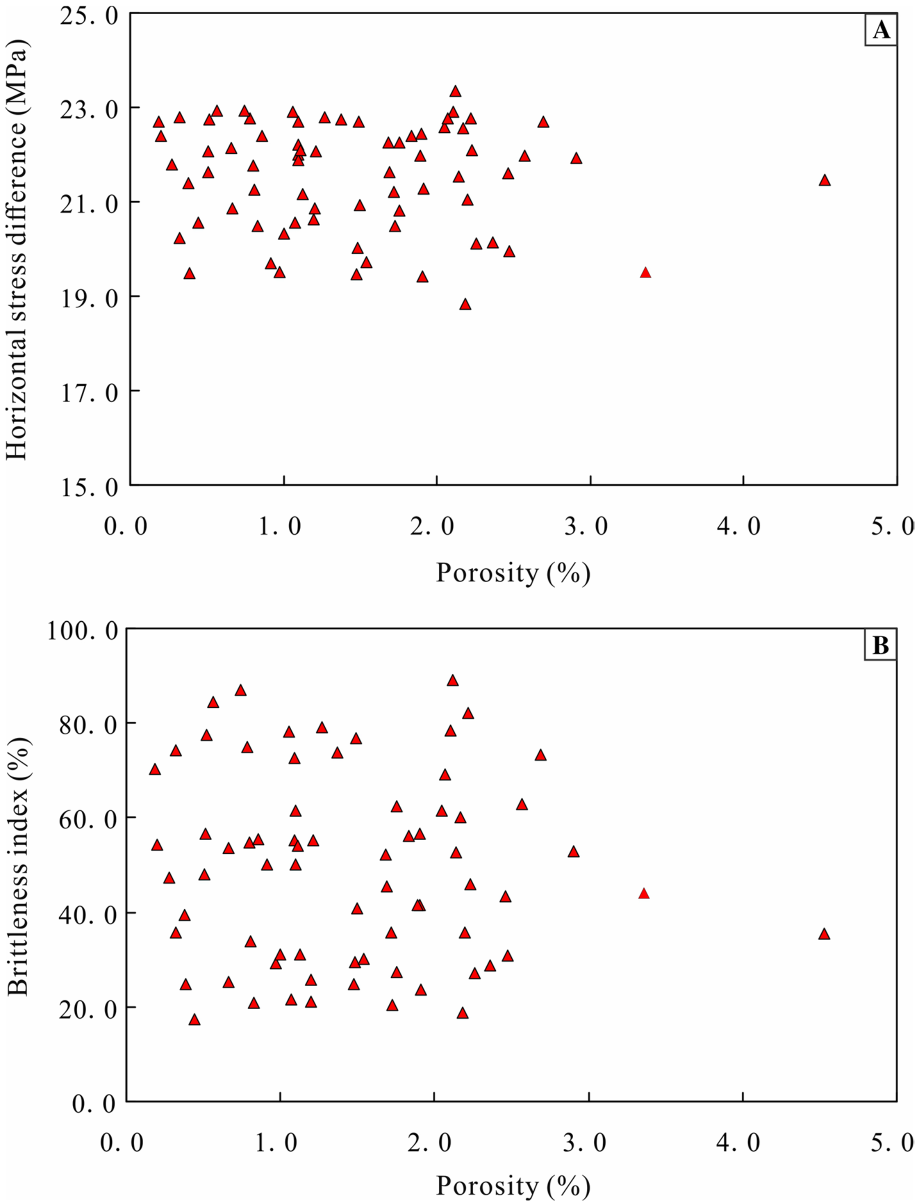

Fig. 23 Crossplots of horizontal stress difference and brittleness index versus porosity in Funing Formation in Subei Basin, East China

well-log responses (Fig. 24). Lithology is predicted by ECS log profile. Then, porosity, permeability and oil saturation are determined from the NMR logs, and NMR T_2 spectrum is also presented to show the fluid bearing property. Additionally, the image logs are used to pick out the fracture traces and derive the in situ stress direction using induced fractures. Consequently, the reservoir property can be evaluated in terms of reservoir quality

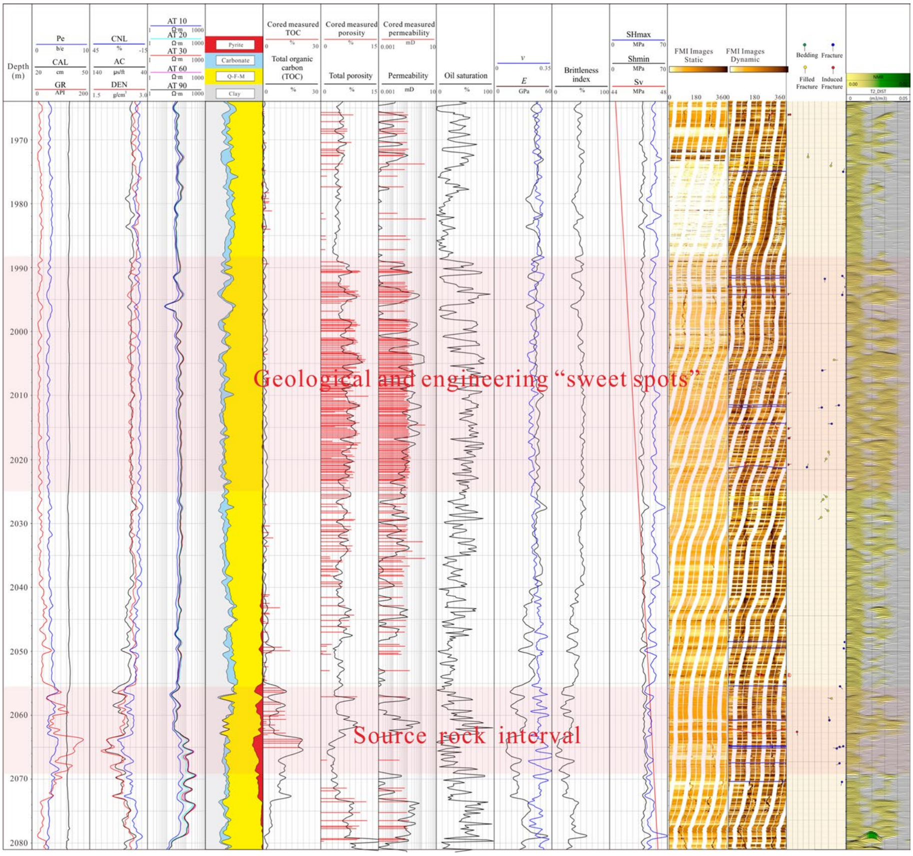

Fig. 24 Comprehensive diagram of the seven types of relationships and three types of properties in Well Cheng 96 in Ordos Basin, West China

(porosity, permeability), oil bearing property (oil saturation and T_2 spectrum) and the presences of natural fractures (Fig. 24). The in situ stress profiles including vertical/overburden stress and maximum/minimum horizontal stress are calculated by density and sonic logs. Brittleness index is determined using Poisson's ratio and Young's modulus (Fig. 24). Additionally, the in situ stress anisotropy profile is generated by picking out the fast shear-wave direction (Fig. 24).

The best source rock intervals are easily recognized by the conventional well logs as well as the calculated TOC content (Fig. 24). The best reservoir property intervals can be distinguished by the wide and high amplitudes of NMR T_2 spectrum. Additionally, the high values of calculated petrophysical parameters of porosity, permeability and oil saturation prove the presences of best reservoir property. Furthermore, the appearances of natural fractures will improve the permeability and form favorable geological sweet spots (Fig. 24). The interconnectivity of the source rock and reservoir is also important for sweet spots in unconventional resources (Kumar et al. 2018; Zhao et al. 2019; Radwan et al. 2021). Therefore, the reservoirs adjacent with the source rock intervals have the best potential for accumulating oil and gas resources (Fig. 24).

The economic production of unconventional reservoirs strongly relies on the hydraulic induced fracture system (Fuentes-Cruz et al. 2014; Iqbal et al. 2018). The direction of stimulation treatments is toward the SH_{max} direction in order to create complex fracture network for oil and gas to flow into the borehole since the hydraulic fractures propagate along SH_{max} (Fig. 17). In addition, the prospected layers optimizing for hydraulic fracturing are those layers with high brittleness index but low horizontal stress differences (Zhang et al. 2017a, b). Layer with high brittleness index (>0.5) but low horizontal stress differences (<15 MPa) are optimized for hydraulic fracturing layers (Fig. 24).

7 Prospects

Geophysical well logs play important roles in the exploration and development of unconventional hydrocarbon resources. However, the high cost of acquiring a comprehensive suite of the required well logs (especially advanced well logs including spectral gamma-ray, NMR, image logs, ECS, etc.) will hinder the application of geophysical well logs in the fields of unconventional hydrocarbon resources. Therefore, the basic suite of well logs should be optimized. Conventional well logs are necessary for source rock property evaluation, and image logs as well as NMR logs need to be logged with the aim for reservoir property evaluation. Array sonic logs and image logs should be optimized for engineering property determination. In addition, the calibration of well-log data with core analysis data will reduce uncertainty, and the optimum sampling of core data will help improve the accuracy of well-log data interpretation.

Geophysical well logs precisely evaluate the petrophysical properties (lithology, porosity, permeability and oil saturation) and geomechanical properties (Poisson's ratio, Young's modulus, brittleness index and in situ stress) of unconventional hydrocarbon resources (Avanzini et al. 2016; Kumar et al. 2018). Consequently, the well logs are widely adopted to answer the key questions in unconventional oil and gas geology and engineering: "Whether there contains abundant oil and gas resources?", "Where are the hydrocarbon reserved?" and "How to optimize the prospected layers for stimulation?". The comprehensive petrophysical approaches will support petroleum geoscientists' and engineers' decisions throughout whole life of unconventional hydrocarbon resources including horizontal drilling, resource assessment, reservoir characterization and hydraulic fracture simulation (Avanzini et al. 2016).

8 Summary and Conclusions

The advanced well-log series used in unconventional oil and gas play evaluation include high definition induction logs, image logs, array acoustic logs, nuclear magnetic resonance (NMR) log, elemental capture spectroscopy (ECS) as well as LithoScanner logs.

Source rock intervals are recognized on the conventional well logs as high GR, low density, high CNL, AC and resistivity values. TOC can be predicted by the $\Delta\log R$ method, spectral GR logs, multivariate fitting method and LithoScanner logs.

Lithology can be predicted by conventional and image logs. Porosity, permeability and oil saturation can be calculated from NMR logs combined with conventional well logs. Fracture can be picked out from the image logs. Reservoir property can be evaluated from the combination of lithology, reservoir quality and the presences of natural fractures. Intervals with high reservoir quality and hydrocarbon bearing property and adjacent with the source rock interval are screened out as the geological sweet spots.

Brittleness can be determined not only from Young's modulus also from rock composition. Brittleness should be well evaluated in terms of fracture initiation and propagation, as well as keeping fracture reopening. Additionally, in situ stress direction and magnitudes also need well understood in terms of horizontal well drilling direction and optimizing propertied hydraulic fracturing intervals. Layers with high brittleness index but low horizontal stress difference are optimized as engineering sweet spots.

Geophysical well logs can characterize the seven kinds of parameters (lithology, reservoir quality, hydrocarbon bearing property, electronic well-log responses, source rock property, brittleness, and in situ stress magnitude and direction) and three kinds of properties (source rock property, reservoir property and engineering property), and therefore will be widely used in optimizing sweet spots in unconventional play in the future.

Acknowledgements This work is financially supported by the National Natural Science Foundation of China (Nos. 42002133, 42072150), Natural Science Foundation of Beijing (8204069), strategic cooperation project of PetroChina and CUPB (China University of Petroleum, Beijing) (ZLZX2020-01-06-01) and Science Foundation of CUPB (No. 2462021YXZZ003). We thank the PetroChina Xinjiang, Tarim, Changqing Oilfield Company for their assistance in providing information, and for their technical input to this work.

References

Aghli G, Soleimani B, Moussavi-Harami R, Mohammadian R (2016) Fractured zones detection using conventional petrophysical logs by differentiation method and its correlation with image logs. J Pet Sci Eng 142:152–162

Amaefule JO, Mehmet A, Djebbar T, David K, Dare K (1993) Enhanced reservoir description: using core and log data to identify hydraulic (flow) unit and predict permeability in uncored intervals/ well, SPE26436, presented at the 68th Annual SPE conference and exhibition, Houston, Texas, 1993

Ameen MS (2014) Fracture and in-situ stress patterns and impact on performance in the khuff structural prospects, eastern offshore Saudi Arabia. Mar Pet Geol 50(50):166–184

Ameen MS, MacPherson K, Al-Marhoon MI, Rahim Z (2012) Diverse fracture properties and their impact on performance in conventional and tight-gas reservoirs, Saudi Arabia: the Unayzah, South Haradh case study. AAPG Bull 96(3):459–492

Amosu A, Sun Y (2021) Identification of thermally mature total organic carbon-rich layers in shale formations using an effective machine-learning approach. Interpretation 9(3):T735–T745

Amosu A, Imsalem M, Sun Y (2021) Effective machine learning identification of TOC-rich zones in the Eagle Ford Shale. J Appl Geophys 188:104311

Anand V (2017) Novel methodology for accurate resolution of fluid signatures from multi-dimensional NMR well-logging measurements. J Magn Reson 276:60–68

Anderson EM (1951) The dynamics of faulting and dyke formation with applications to Britain. Oliver and Boyd, Edinburgh

Assousa S, Elkington P (2014) Phase-based dispersion analysis for acoustic array borehole logging data. J Acoust Soc Am 135(4):1919–1928

Avanzini A, Balossino P, Brignoli M, Spelta E, Tarchiani C (2016) Lithologic and geomechanical facies classification for sweet spot identification in gas shale reservoir. Interpretation 4(3):SL21–SL31

Aziz H, Ehsan M, Ali A, Khan HK, Khan A (2020) Hydrocarbon source rock evaluation and quantification of organic richness from correlation of well logs and geochemical data: a case study from the sembar formation, Southern Indus Basin, Pakistan. J Nat Gas Sci Eng 81:103433

Bai H, Pang X, Kuang L, Pang H, Wang X, Jia X, Zhou L, Hu T (2017) Hydrocarbon expulsion potential of source rocks and its influence on the distribution of lacustrine tight oil reservoir, Middle

Permian Lucaogou Formation, Jimsar Sag, Junggar Basin, Northwest China. J Petrol Sci Eng 149:740–755
Basa A, Ahmed F, Bhattacharyya K, Roy A (2019) Evolution and characterization of fracture patterns: insights from multi-scale analysis of the Buxa dolomite in the Siang Valley, Arunachal Lesser Himalayan fold-thrust belt. J Struct Geol 123:54–66
Bauer K, Kulenkampff J, Henninges J, Spangenberg E (2015) Lithological control on gas hydrate saturation as revealed by signal classification of NMR logging data. J Geophys Res Solid Earth 120:6001–6017
Cao Z, Liu G, Zhan H, Gao J, Zhang J, Li C, Xiang B (2017) Geological roles of the siltstones in tight oil play. Mar Pet Geol 83:333–344
Chandra D, Vishal V (2021) A critical review on pore to continuum scale imaging techniques for enhanced shale gas recovery. Earth Sci Rev 217:103638
Chen Z, Lavoie D, Malo M, Jiang C, Sanei H, Ardakani OH (2017) A dual-porosity model for evaluating petroleum resource potential in unconventional tight-shale plays with application to Utica Shale, Quebec (Canada). Mar Pet Geol 80:333–348
Clarkson CR (2013) Production data analysis of unconventional gas wells: workflow. Int J Coal Geol 109–110:147–157
Clarkson CR, Jensen JL, Chipperfield S (2012) Unconventional gas reservoir evaluation: What do we have to consider? J Nat Gas Sci Eng 8:9–33
Coates GR, Xiao L, Prammer MG (1999) NMR logging, principle and applications. Halliburton, Houston
Collett TS, Lewis RE, Winters WJ, Lee MW, Rose KK, Boswell RM (2011) Downhole well log and core montages from the mount elbert gas hydrate stratigraphic test well, Alaska north slope. Mar Pet Geol 28:561–577
Curtis JB (2002) Fractured shale-gas systems. AAPG Bull 86(11):1921–1938
Curtis ME, Cardott BJ, Sondergeld CH, Rai CS (2012) Development of organic porosity in the Woodford Shale with increasing thermal maturity. Int J Coal Geol 103:26–31
Deng F, Xiao L, Chen W, Liu H, Liao G, Wang M, Xie Q (2014) Rapid determination of fluid viscosity using low-field two-dimensional NMR. J Magn Reson 247:1–8
Doveton JH (2014) Compositional analysis of mineralogy. In: Principles of mathematical petrophysics. Oxford University Press. https://scholar.google.com.sg/scholar?q=Compositional+analysis+of+mineralogy.+In:+Principles+of+mathematical+petrophysics&hl=zh-CN&as_sdt=0&as_vis=1&oi=scholart
Dixit NC, Hanks CL, Wallace WK, Ahmadi M, Awoleke O (2017) In situ stress variations associated with regional changes in tectonic setting, northeastern Brooks Range and eastern North Slope of Alaska. AAPG Bull 101(3):343–360
Dong T, Harris NB, Knapp LJ, McMillan JM, Bish DL (2018) The effect of thermal maturity on geomechanical properties in shale reservoirs: an example from the Upper Devonian Duvernay Formation, Western Canada Sedimentary Basin. Mar Pet Geol 97:137–153
Du B, Zhang G, Zhang J, Gao J, Yong X, Yang W, Jiang R, Wang S, Li H, Wang E (2021) Stress prediction and evaluation approach based on azimuthal amplitude-versus-offset inversion of unconventional reservoirs. Geophys Prospect 69:372–387
Dunn KJ, Bergman DJ, LaTorraca GA (eds) (2002) Nuclear magnetic resonance: petrophysical and logging applications. Elsevier. https://scholar.google.com.sg/scholar?hl=zh-CN&as_sdt=0%2C5&as_vis=1&q=Nuclear+magnetic+resonance%3A+petrophysical+and+logging+applications&btnG=
Engelder T (1993) Stress regimes in the lithosphere. Princeton University Press, New Jersey
Fan X, Su JZ, Chang X, Huang ZW, Zhou T, Guo YT, Wu SQ (2019) Brittleness evaluation of the inter-salt shale oil reservoir in Jianghan Basin in China. Mar Pet Geol 102:109–115
Folkestad A, Veselovsky Z, Roberts P (2012) Utilising borehole image logs to interpret delta to estuarine system: a case study of the subsurface Lower Jurassic cook formation in the Norwegian northern North Sea. Mar Pet Geol 29:255–275
Fuentes-Cruz G, Gildin E, Valkó PP (2014) On the analysis of production data: practical approaches for hydraulically fractured wells in unconventional reservoirs. J Petrol Sci Eng 119:54–68
Gale JFW, Reed RM, Holder J (2007) Natural fractures in the Barnett Shale and their importance for hydraulic fracture treatments. AAPG Bull 91(4):603–622
Gale JFW, Laubach SE, Olson JE, Eichhubl P, Fall A (2014) Natural fractures in shale: a review and new observations. AAPG Bull 98(11):2165–2216
Gao G, Zhang W, Xiang B, Liu G, Ren J (2016) Geochemistry characteristics and hydrocarbon-generating potential of lacustrine source rock in Lucaogou Formation of the Jimusaer Sag, Junggar Basin. J Petrol Sci Eng 145:168–182
Gholami R, Rasouli V, Sarmadivaleh M, Minaeian V, Fakhari N (2016) Brittleness of gas shale reservoirs: a case study from the north Perth basin, Australia. J Nat Gas Sci Eng 33:1244–1259

Glover PWJ, Zadjali II, Frew KA (2006) Permeability prediction from MICP and NMR data using an electrokinetic approach. Geophysics 71(4):F49–F60
Godfray G, Seetharamaiah J (2019) Geochemical and well logs evaluation of the Triassic source rocks of the Mandawa basin, SE Tanzania: implication on richness and hydrocarbon generation potential. J Afr Earth Sci 153:9–16
Goodall TM, Moller NK, Ronningsland TM (1998) The integration of electrical image logs 237 with core data for improved sedimentological interpretation. Geol Soc Lond Spec Publ 136:237–248
Guo T, Zhang S, Ge H, Wang X, Lei X, Xiao B (2015) A new method for evaluation of fracture network formation capacity of rock. Fuel 140:778–787
Guo P, Liu C, Wang L, Zhang G, Fu X (2019) Mineralogy and organic geochemistry of the terrestrial lacustrine pre-salt sediments in the Qaidam Basin: implications for good source rock development. Mar Pet Geol 107:149–162
Guo J, Xie R, Xiao L (2020) Pore-fluid characterizations and microscopic mechanisms of sedimentary rocks with three-dimensional NMR: tight sandstone as an example. J Nat Gas Sci Eng 80:103392
He J, Croix ADL, Wang J, Ding W, Underschultz JR (2019) Using neural networks and the Markov Chain approach for facies analysis and prediction from well logs in the Precipice Sandstone and Evergreen Formation, Surat Basin, Australia. Mar Pet Geol 101:410–427
Henares S, Caracciolo L, Viseras C, Fernandez J, Yeste LM (2016) Diagenetic constraints on heterogeneous reservoir quality assessment: a Triassic outcrop analog of meandering fluvial reservoirs. AAPG Bull 100(9):1377–1398
Hooker JN, Cartwright J, Stephenson B, Silver CRP, Dickson AJ, Hsieh YT (2017) Fluid evolution in fracturing black shales, Appalachian Basin. AAPG Bull 101(8):1203–1238
Hsieh BZ, Lewis C, Lin Z (2005) Lithology identification of aquifers from geophysical well logs and fuzzy logic analysis: Shui-Lin Area, Taiwan. Comput Geosci 31:263–275
Huang W, Lu S, Osman SH (2017) Quality grading system for tight sandstone reservoirs in the Quantou 4 member, southern Songliao Basin, Northeast China. Interpretation 5(4):1–20
Hübner W (2014) Studying the pore space of cuttings by NMR and μCT. J Appl Geophys 104:97–105
Iqbal O, Ahmad M, Kadir A (2018) Effective evaluation of shale gas reservoirs by means of an integrated approach to petrophysics and geomechanics for the optimization of hydraulic fracturing: a case study of the Permian Roseneath and Murteree Shale Gas reservoirs, Cooper Basin, Australia. J Nat Gas Scie Eng 58:34–58
Jarvie DM, Hill RJ, Ruble TE (2007) Unconventional shale-gas systems: the Mississippian Barnett Shale of north-central Texas as one model for thermogenic shale-gas assessment. AAPG Bull 91:475–499
Josh M, Esteban L, Delle PC, Sarout J, Dewhurst DN, Clennell MB (2012) Laboratory characterisation of shale properties. J Petrol Sci Eng 88–89:107–124
Keeton G, Pranter M, Cole RD, Gustason ER (2015) Stratigraphic architecture of fluvial deposits from borehole images, spectral-gamma-ray response, and outcrop analogs, Piceance Basin, Colorado. AAPG Bull 99(10):1929–1956
Khoshbakht F, Memarian H, Mohammadnia M (2009) Comparison of Asmari, Pabdeh and Gurpi formation's fractures, derived from image log. J Petrol Sci Eng 67:65–74
Khoshbakht F, Azizzadeh M, Memarian H, Nourozi GH, Moallemi SA (2012) Comparison of electrical image log with core in a fractured carbonate reservoir. J Pet Sci Eng 86–87:289–296
Kleinberg RL, Flaum C, Collett TS (2005) Magnetic resonance log of JAPEX/JNOC/GSC et al. Mallik 5L-38 gas hydrate production research well: gas hydrate saturation, growth habit, and relative permeability. In: Dallimore SR, Collett TS (eds) Scientific results from the Mallik 2002 gas hydrate production research well program, Mackenzie Delta, Northwest Territories, Canada, Bull. Geol. Surv. of Canada, Ottawa, Canada, 10
Khair HA, Cooke D, Hand M (2013) The effect of present day in situ stresses and paleo-stresses on locating sweet spots in unconventional reservoirs, a case study from Moomba-Big Lake fields, Cooper Basin, South Australia. J Pet Explor Prod Technol 3:207–221
Khair HA, Cooke D, Hand M (2015) Paleo stress contribution to fault and natural fracture distribution in the Cooper Basin. J Struct Geol 79:31–41
Kingdon A, Fellgett MW, Williams JDO (2016) Use of borehole imaging to improve understanding of the in-situ stress orientation of Central and Northern England and its implications for unconventional hydrocarbon resources. Mar Pet Geol 73:1–20
Kumar S, Das S, Bastia R, Ojha K (2018) Mineralogical and morphological characterization of Older Cambay Shale from North Cambay Basin, India: Implication for shale oil/gas development. Mar Pet Geol 97:339–354

Ladevèze P, Séjournéc S, Rivardb C, Lavoieb D, Lefebvrea RRA (2018) Defining the natural fracture network in a shale gas play and its cover succession: the case of the Utica Shale in eastern Canada. J Struct Geol 108(2018):157–170
Lai J, Wang G, Huang L, Li W, Ran Y, Wang D, Zhou Z, Chen J (2015) Brittleness index estimation in a tight shaly sandstone reservoir using well logs. J Nat Gas Sci Eng 27:1536–1545
Lai J, Wang G, Fan Z, Chen J, Wang S, Zhou Z, Fan X (2016) Insight into the pore structure of tight sandstones using NMR and HPMI measurements. Energy Fuels 30:10200–10214
Lai J, Wang G, Fan Z, Wang Z, Chen J, Zhou Z, Wang S, Xiao C (2017) Fracture detection in oil-based drilling mud using a combination of borehole image and sonic logs. Mar Pet Geol 84:195–214
Lai J, Wang G, Wang S, Cao J, Li M, Pang X, Han C, Fan X, Yang L, He Z, Qin Z (2018a) A review on the applications of image logs in structural analysis and sedimentary characterization. Mar Pet Geol 95:139–166
Lai J, Wang G, Wang Z, Chen J, Pang X, Wang S, Zhou Z, He Z, Qin Z, Fan X (2018b) A review on pore structure characterization in tight sandstones. Earth Sci Rev 177:436–457
Lai J, Li D, Wang G, Xiao C, Hao X, Luo Q, Lai L, Qin Z (2019) Earth stress and reservoir quality evaluation in high and steep structure: The Lower Cretaceous in the Kuqa Depression, Tarim Basin, China. Mar Pet Geol 101:43–54
Lai J, Liu S, Xin Y, Wang S, Xiao C, Song Q, Chen X, Wang G, Qin Z, Ding X (2021) Geological-petrophysical insights in the deep Cambrian dolostone reservoirs in Tarim Basin, China. AAPG Bull 105(11):2263–2296
Lai J, Fan X, Li Y, Zhao X, Liu S, Liu X, Li D, Pang X, Li H, Luo Y (2022) Well logging evaluation of seven kinds of relationships and three types of properties of Paleogene Funing Formation oil shales in Subei Basin. Geol Rev 68(2):751–768
Lee HP, Olson JE, Holder J, Gale JFW, Myers RD (2015) The interaction of propagating opening mode fractures with preexisting discontinuities in shale. J Geophys Res Solid Earth 120:169–181
Li JZ, Laubach SE, Gale JFW, Marrett RA (2018) Quantifying opening-mode fracture spatial organization in horizontal wellbore image logs, core and outcrop: application to upper cretaceous frontier formation tight gas sandstones, USA. J Struct Geol 108:137–156
Li M, Chen Z, Ma X, Cao T, Qian M, Jiang Q, Tao G, Li Z, Song G (2019) Shale oil resource potential and oil mobility characteristics of the Eocene-Oligocene Shahejie Formation, Jiyang Super-Depression, Bohai Bay Basin of China. Int J Coal Geol 204:130–143
Li YE, Cheng ACH, You N (2019) Shale anisotropy estimation from logs in vertical wells. J Geophys Res Solid Earth 124:6602–6611
Li J, Jiang C, Wang M, Lu S, Chen Z, Chen G, Li J, Li Z, Lu S (2020) Adsorbed and free hydrocarbons in unconventional shale reservoir: a new insight from NMR T1–T2 maps. Mar Pet Geol 116:104311
Li Y, Hu Z, Cai C, Liu X, Duan X, Chang J, Li Y, Mu Y, Zhang Q, Zeng S, Guo J (2021) Evaluation method of water saturation in shale: a comprehensive review. Mar Pet Geol 128:105017
Liang M, Wang Z, Zhang Y, Greenwell CH, Li H, Yu Y, Liu S (2021) Experimental investigation on gas permeability in bedding shale with brittle and semi-brittle deformations under triaxial compression. J Pet Sci Eng 196:108049
Liu G (2021) Challenges to log evaluation in unconventional petroleum era and countermeasures. Pet Explor Dev 48(5):1–12
Liu J, Ding W, Wang R, Yang H, Wang X, Li A (2018) Correlation analysis of element contents and mechanical characteristics of shale reservoirs: a case study in the Cen'gong block, South China. Mar Pet Geol 91:19–28
Liu J, Fan Y, Qiu T, Ge X, Deng S, Xing D (2019) A novel pulse sequence and inversion algorithm of three-dimensional low field NMR technique in unconventional resources. J Magn Reson 303:67–74
Liu X, Lai J, Fan X, Shu H, Wang G, Ma X, Liu M, Guan M, Luo Y (2020) Insights in the pore structure, fluid mobility and oiliness in oil shales of Paleogene Funing Formation in Subei Basin, China. Mar Pet Geol 114:104228
Liu X, Jin Z, Lai J, Fan X, Guan M, Shu H, Wang G, Liu M, Luo Y (2021) Fractal behaviors of NMR saturated and centrifugal T_2 spectra in oil shale reservoirs: the Paleogene Funing formation in Subei basin, China. Mar Pet Geol 129:105069
Loucks RG, Reed RM, Ruppel SC, Hammes U (2012) Spectrum of pore types and networks in mudrocks and a descriptive classification for matrix-related mudrock pores. AAPG Bull 96:1071–1098
Lu M, Cao H, Sun W, Yan X, Yang Z, Xu Y, Wang Z, Ouyang M (2019) Quantitative prediction of seismic rock physics of hybrid tight oil reservoirs of the Permian Lucaogou Formation, Junggar Basin, Northwest China. J Asian Earth Sci 178:216–223

Mahmoud AAA, Elkatatny S, Mahmoud M, Abouelresh M, Abdulraheem A, Ali A (2017) Determination of the total organic carbon (TOC) based on conventional well logs using artificial neural network. Int J Coal Geol 179:72–80
Maleki S, Moradzadeh A, Riabi RG, Sadaghzadeh F (2014) Comparison of several different methods of in situ stress determination. Int J Rock Mech Min Sci 71(71):395–404
Maliva RG, Clayton EA, Missimer TM (2009) Application of advanced borehole geophysical logging to managed aquifer recharge investigations. Hydrogeol J 17(6):1547–1556
Manjunath GL, Jha B (2019) Geomechanical characterization of gondwana shale across nano-micro-meso scales. Int J Rock Mech Min Sci 119:35–45
Massiot C, Mcnamara DD, Lewis B (2015) Processing and analysis of high temperature geothermal acoustic borehole image logs in the Taupo volcanic zone, New Zealand. Geothermics 53:190–201
McGinnis RN, Ferrill DA, Morris AP, Smart KJ, Lehrmann D (2017) Mechanical stratigraphic controls on natural fracture spacing and penetration. J Struct Geol 95:160–170
Mews KS, Alhubail MM, Barati RG (2019) A review of brittleness index correlations for unconventional tight and ultra-tight reservoirs. Geosciences 2019(9):319
Mukhametdinova A, Habina-Skrzyniarz I, Kazak A, Krzyzak A (2021) NMR relaxometry interpretation of source rock liquid saturation—a holistic approach. Mar Pet Geol 132:105165
Nhabanga OJ, Ringrose PS, Holt RM (2021) Use of rock-physics analysis of well logs to determine compaction history of Cretaceous shales in the Rovuma basin, Offshore Mozambique. Geophys Prospect 69:1282–1294
Nian T, Wang G, Xiao C, Zhou L, Deng L, Li R (2016) The in situ stress determination from borehole image logs in the Kuqa Depression. J Nat Gas Sci Eng 34:1077–1084
Nikolaev MY, Kazak AV (2019) Liquid saturation evaluation in organic-rich unconventional reservoirs: a comprehensive review. Earth Sci Rev 194:327–349
Olatinsu OB, Olorode DO, Clennell B, Esteban L, Josh M (2017) Lithotype characterizations by nuclear magnetic resonance (NMR): A case study on limestone and associated rocks from the Eastern Dahomey basin, Nigeria. J Afr Earth Sc 129:701–712
Passey Q, Creaney S, Kulla J, Moretti F, Stroud J (1990) A practical model for organic richness from porosity and resistivity logs. AAPG Bull 74:1777–1794
Prioul R, Donald A, Koepsell R, Marzouki ZE, Bratton T (2007) Forward modeling of fracture-induced sonic anisotropy using a combination of borehole image and sonic logs. Geophysics 72(4):135–147
Qian K, Liu T, Liu J, Liu X, He Z, Jiang D (2020) Construction of a novel brittleness index equation and analysis of anisotropic brittleness characteristics for unconventional shale formations. Pet Sci 17:70–85
Qiu Z, Tao H, Zou C, Wang H, Ji H, Zhou S (2016) Lithofacies and organic geochemistry of the Middle Permian Lucaogou Formation in the Jimusar Sag of the Junggar Basin, NW China. J Pet Sci Eng 140:97–107
Radwan AE, Trippetta F, Kassem AA, Kania M (2021) Multi-scale characterization of unconventional tight carbonate reservoir: insights from October oil filed, Gulf of Suez rift basin, Egypt. J Pet Sci Eng 197:107968
Rajabi M, Sherkati S, Bohloli B, Tingay M (2010) Subsurface fracture analysis and determination of in-situ stress direction using FMI logs: an example from the Santonian carbonates (Ilam Formation) in the Abadan Plain, Iran. Tectonophysics 492:192–200
Ran Y, Wang G, Zhou Z, Lai J, Dai Q, Chen J, Fan X, Wang S (2016) Identification of lithology and lithofacies type and its application to Chang 7 tight oil in Heshui area, Ordos Basin. Geol China 43(4):1331–1340 (**in Chinese with English abstract**)
Rezaee R, Saeedi A, Clennell B (2012) Tight gas sands permeability estimation from mercury injection capillary pressure and nuclear magnetic resonance data. J Petrol Sci Eng 88–89:92–99
Rickman R, Mullen MJ, Petre JE, Grieser B, Kundert D (2008) A practical use of shale petrophysics for stimulation design optimization: all shale plays are not clones of the Barnett Shale. In: SPE annual technical conference and exhibition. Society of Petroleum Engineers
Rybacki E, Reinicke A, Meier T, Makasi M, Dresen G (2015) What controls the mechanical properties of shale rocks?—part I: strength and young's modulus. J Petrol Sci Eng 135:702–722
Rybacki E, Meier T, Dresen G (2016) What controls the mechanical properties of shale rocks?—Part II: brittleness. J Petrol Sci Eng 144:39–58
Schmid S, Worden RH, Fisher Q (2004) Diagenesis and reservoir quality of the Sherwood Sandstone (Triassic), Corrib Field, Slyne Basin, West of Ireland. Marine Petrol Geol 21:299–315

Sérgio SLR, Duarte LV, Pereira AJSC, Silva RL (2018) Field gamma-ray patterns and stratigraphic reinterpretation of offshore well-log data from Lower Jurassic organic-rich units of the Lusitanian Basin (Portugal). Mar Pet Geol 98:860–872

Shalaby MR, Jumat N, Lai D, Malik O (2019) Integrated TOC prediction and source rock characterization using machine learning, well logs and geochemical analysis: Case study from the Jurassic source rocks in Shams Field, NW Desert, Egypt. J Pet Sci Eng 176:369–380

Soliman MY, Kabir CS (2012) Testing unconventional formations. J Petrol Sci Eng 92–93:102–109

Sondergeld CH, Newsham KE, Comisky JT et al (2010) Petrophysical considerations in evaluating and producing shale gas resources. In: SPE Unconventional Gas Conference. Society of Petroleum Engineers

Su Y, Zha M, Ding XJ et al (2018) Pore type and pore size distribution of tight reservoirs in the permian Lucaogou Formation of the Jimsar sag, Junggar Basin, NW China. Mar Pet Geol 89(23):761–774

Su Y, Zha M, Ding X, Qu J, Gao C, Jin J, Iglauer S (2019) Petrographic, palynologic and geochemical characteristics of source rocks of the Permian Lucaogou formation in Jimsar Sag, Junggar Basin, NW China: Origin of organic matter input and depositional environments. J Pet Sci Eng 183:106364

Sun BQ, Dunn KJ (2005) Two-dimensional nuclear magnetic resonance petrophysics. Magn Reson Imaging 23(2):259–262

Sun Y, Chen S, Li Y, Zhang J, Gong F (2021) Shale rocks brittleness index prediction method using extended elastic impedance inversion. J Appl Geophys 188:104314

Stadtmuller M, Lis-Sledziona A, Słota-Valim M (2018) Petrophysical and geomechanical analysis of the Lower Paleozoic shale formation, North Poland. Interpretation 6(3):SH91–SH106

Tan M, Wang P, Mao K (2014) Comparative study of inversion methods of three-dimensional NMR and sensitivity to fluids. J Appl Geophys 103(4):12–30

Tenaglia M, Eberli GP, Weger RJ, Blanco LR, Sanchez LER, Swart PK (2020) Total organic carbon quantification from wireline logging techniques: a case study in the Vaca Muerta Formation, Argentina. J Pet Sci Eng 194:107489

Verma S, Zhao T, Marfurt K, Devegowda D (2016) Estimation of total organic carbon and brittleness volume. Interpretation 4(3):T373–T385

Verweij JM, Boxem TAP, Nelskamp S (2016) 3D spatial variation in vertical stress in on- and offshore Netherlands; integration of density log measurements and basin modeling results. Mar Pet Geol 78:870–882

Venieri M, Harazim D, Pedersen PK, Eaton DW (2021) Vertical and lateral facies variability in organic-rich mudstones at the reservoir scale: a case study from the Devonian Duvernay formation of Alberta Canada. Mar Petr Geol 132:105232

Wang H, Wu W, Chen T, Dong X, Wang G (2019) An improved neural network for TOC, S1 and S2 estimation based on conventional well logs. J Petrol Sci Eng 176:664–678

Wang W, Zhao Y, Mao R, Sun Z, Mu L (2019) Determination of the starting time for measurement of NMR effective porosity in shale oil reservoir: a case study of the Permian Lucaogou shale oil reservoir Jimusaer sag. Oil Gas Geol 40(3):550–557

Wang S, Wang G, Lai J, Li D, Liu S, Chen X, Yang K, Song L (2020) Logging identification and evaluation of vertical zonation of buried hill in Cambrian dolomite reservoir: a study of Yingmai-Yaha buried hill structural belt, northern Tarim basin. J Pet Sci Eng 195:107758

Wang G, Lai J, Liu B, Fan Z, Liu S, Shi Y, Zhang H, Chen J (2020) Fluid property discrimination in dolostone reservoirs using well logs. Acta Geol Sin (engl Edn) 94(3):831–846

Wang S, Wang G, Huang L, Song L, Zhang Y, Li D, Huang Y (2021) Logging evaluation of lamina structure and reservoir quality in shale oil reservoir of Fengcheng Formation in Mahu Sag, China. Mar Pet Geol 133:105299

Wilson MEJ, Lewis D, Yogi O, Holland D, Hombo L, Goldberg A (2013) Development of a Papua New Guinean onshore carbonate reservoir: a comparative borehole image (BHI) and petrographic evaluation. Mar Pet Geol 44:164–195

Wood DA (2020a) Total organic carbon predictions from lower Barnett shale well-log data applying an optimized data matching algorithm at various sampling densities. Pure Appl Geophys 177:5451–5468

Wood DA (2020b) Predicting porosity, permeability and water saturation applying an optimized nearest-neighbour, machine-learning and data-mining network of well-log data. J Pet Sci Eng 184:106587

Wood DA (2021) Brittleness index predictions from Lower Barnett Shale well-log data applying an optimized data matching algorithm at various sampling densities. Geosci Front 12:101087

Wu H, Hu W, Tang Y, Cao J, Wang X, Wang Y, Kang X (2017) The impact of organic fluids on the carbon isotopic compositions of carbonate-rich reservoirs: case study of the Lucaogou Formation in the Jimusaer Sag, Junggar Basin, NW China. Mar Pet Geol 85:136–150

Wu S, Zhai X, Yang Z, Bale H, Hong Y, Cui J, Pan S, Lin S (2019) Characterization of fracture formation in organic-rich shales—an experimental and real time study of the Permian Lucaogou Formation, Junggar Basin, northwestern China. Mar Pet Geol 107:397–406
Xi K, Cao Y, Liu K, Jahren J, Zhu R, Yuan G, Hellevang H (2019) Authigenic minerals related to wettability and their impacts on oil accumulation in tight sandstone reservoirs: an example from the Lower Cretaceous Quantou Formation in the southern Songliao Basin, China. J Asian Earth Sci 178:173–192
Xu C, Cronin TP, McGinness TE, Steer B (2009) Middle Atokan sediment gravity flows in the Red Oak field, Arkoma Basin, Oklahoma: a sedimentary analysis using electrical borehole images and wireline logs. AAPG Bull 93(1):1–29
Xu S, Gou Q, Hao F, Zhang B, Shu Z, Zhang Y (2020) Multiscale faults and fractures characterization and their effects on shale gas accumulation in the Jiaoshiba area, Sichuan Basin, China. J Pet Sci Eng 189:107026
Yang Z, Zou C, Hou L, Wu S, Lin S, Luo X, Zhang L, Zhao Z, Cui J, Pan S (2019) Division of fine-grained rocks and selection of "sweet sections" in the oldest continental shale in China: taking the coexisting combination of tight and shale oil in the Permian Junggar Basin. Mar Pet Geol 109:339–348
Yarmohammadi S, Kadkhodaie A, Hosseinzadeh S (2020) An integrated approach for heterogeneity analysis of carbonate reservoirs by using image log based porosity distributions, NMR T_2 curves, velocity deviation log and petrographic studies: a case study from the South Pars gas field, Persian Gulf Basin. J Pet Sci Eng 192:107283
Yawar Z, Schieber J (2017) On the origin of silt laminae in laminated shales. Sed Geol 360:22–23
Zhang C, Zhu D, Luo Q, Liu L, Liu D, Yan L, Zhang Y (2017a) Major factors controlling fracture development in the Middle Permian Lucaogou Formation tight oil reservoir, Junggar Basin, NW China. J Asian Earth Sci 146:279–295
Zaree V, Riahi MA, Khoshbakht F, Hemmati HR (2016) Estimating fracture intensity in hydrocarbon reservoir: an approach using DSI data analysis. Carbonates Evaporites 31:101–107
Zazoun RS (2013) Fracture density estimation from core and conventional well logs data using artificial neural networks: the Cambro-Ordovician reservoir of Mesdar oil field, Algeria. J Afr Earth Sci 83:55–73
Zeng L, Li X (2009) Fractures in sandstone reservoirs with ultra-low permeability: a case study of the Upper Triassic Yanchang Formation in the Ordos Basin, China. AAPG Bull 93(4):461–477
Zeng L, Lyu W, Li J, Zhu L, Weng J, Yue F, Zu K (2016) Natural fractures and their influence on shale gas enrichment in Sichuan Basin, China. J Nat Gas Sci Eng 30:1–9
Zhang Y, Pe-Piper G, Piper DJW (2015) How sandstone porosity and permeability vary with diagenetic minerals in the Scotian Basin, offshore Eastern Canada: implications for reservoir quality. Mar Pet Geol 63:28–45
Zhang D, Ranjith PG, Perera MSA (2016) The brittleness indices used in rock mechanics and their application in shale hydraulic fracturing: a review. J Petrol Sci Eng 143:158–170
Zhang S, Huang H, Dong Y, Yang X, Wang C, Luo Y (2017b) Direct estimation of the fluid properties and brittleness via elastic impedance inversion for predicting sweet spots and the fracturing area in the unconventional reservoir. J Nat Gas Sci Eng 45:415–427
Zhang S, Yan J, Cai J, Zhu X, Hu Q, Wang M, Geng B, Zhong G (2021a) Fracture characteristics and logging identification of lacustrine shale in the Jiyang depression, Bohai Bay Basin, Eastern China. Mar Pet Geol 132:105192
Zhang X, Wei B, You J, Liu J, Wang D, Lu J, Tong J (2021b) Characterizing pore-level oil mobilization processes in unconventional reservoirs assisted by state-of-the-art nuclear magnetic resonance technique. Energy 236:121549
Zhao P, Mao Z, Huang Z, Zhang C (2016) A new method for estimating total organic carbon content from well logs. AAPG Bull 100(8):1311–1327
Zhao P, Ostadhassan M, Shen B, Liu W, Abarghani A, Liu K, Luo M, Cai J (2019) Estimating thermal maturity of organic-rich shale from well logs: case studies of two shale plays. Fuel 235:1195–1206
Zhao X, Zhou L, Pu X, Han W, Jin F, Xiao D, Shi Z, Deng Y, Zhang W, Jiang W (2019) Exploration breakthroughs and geological characteristics of continental shale oil: A case study of the Kongdian Formation in the Cangdong Sag, China. Mar Pet Geol 102:544–556
Zhao P, Fu J, Shi Y, Li G, Ostadhassan M, Luo M, Mao Z (2020) Hydrocarbon saturation in shale oil reservoirs by inversion of dielectric dispersion logs. Fuel 266:116934
Zoback M, Barton C, Brudy M, Castillo D, Finkbeiner T, Grollimund B, Moos D, Peska P, Ward C, Wiprut D (2003) Determination of stress orientation and magnitude in deep wells. Int J Rock Mech Min Sci 40:1049–1076

Zou CN, Yang Z, Tao SZ, Yuan X, Zhu R, Hou LWuS, Sun L, Zhang GS, Bai B, Wang L, Gao X, Pang Z (2013) Continuous hydrocarbon accumulation over a large area as a distinguishing characteristic of unconventional hydrocarbon, Ordos Basin. Earth Sci Rev 126:358–369

Zou C, Zhu R, Chen Z, Ogg JG, Wu S, Dong D, Qiu Z, Wang Y, Wang L, Lin S, Cui J, Su L, Yang Z (2019) Organic-matter-rich shales of China. Earth Sci Rev 189:51–78

Authors and Affiliations

Jin Lai[1,2] · Guiwen Wang[1,2] · Qixuan Fan[2] · Xiaojiao Pang[2] · Hongbin Li[2] · Fei Zhao[2] · Yuhang Li[2] · Xin Zhao[2] · Yidi Zhao[2] · Yuyue Huang[2] · Meng Bao[2] · Ziqiang Qin[3] · Qiqi Wang[4]

Guiwen Wang
wanggw@cup.edu.cn

1 State Key Laboratory of Petroleum Resources and Prospecting, China University of Petroleum (Beijing), Beijing 102249, China

2 College of Geosciences, China University of Petroleum (Beijing), Beijing 102249, China

3 Department of Petroleum Engineering, University of Wyoming, Laramie, WY 82071-2000, USA

4 Bureau of Economic Geology, Jackson School of Geosciences, The University of Texas at Austin, Austin, TX 78713-8924, USA